https://doi.org/10.5194/egusphere-2023-74
Preprint. Discussion started: 6 February 2023

The marine methane cycle in the Canadian Arctic Archipelago during summer.

Alessandra D'Angelo[1], Cynthia Garcia-Eidell[2], Zak Kerringan[1], Jacob Strock[1], Frances Crable[2], Nikolas VanKeersbilck[3], Humair Raziuddin[2], Theressa Ewa[2], Samira Umar[2], Andrew L. King[4], Miquel Gonzelez-Meler[2] and Brice Loose[1]

[1]University of Rhode Island, Graduate School of Oceanography, Narragansett, RI 02882, USA
[2]University of Illinois at Chicago, Chicago, IL 60607, USA
[3]University of Iceland, 102 Reykjavík, Iceland
[4]Norwegian Institute for Water Research, 0579 Oslo, Norway

Corresponding author: Alessandra D'Angelo, a_dangelo@uri.edu

Abstract

In the Arctic Ocean region, methane concentrations are higher than the global average; high concentrations of dissolved CH_4 are detectable especially across many subarctic and Arctic continental shelf margins. Yet the Arctic Ocean appears to emit only minimal methane fluxes to the atmosphere across the air-sea interface, suggesting water column oxidation of methane may be an important process. Here we paired thermohaline, chemical, and biological data collected during the Northwest Passage Project transit through the Canadian Arctic Archipelago (CAA) waters in the Summer of 2019, with in-situ and in-vitro methane data. Our results showed high meltwater (meteoric water + sea ice melt) throughout the Western CAA and Croker Bay in the East, and these surface meltwaters showed methane excess. The meteoric waters showed a strong correlation with chlorophyll-α fluorescence (r=0.63), as well as a correlation between dissolved [CH_4] and chlorophyll-α fluorescence (r=0.74). Methane oxidation rate constants were highest in Wellington Channel and Croker Bay surface waters (av. 0.01±0 d^{-1}), characterized by meltwaters and Pacific-origin waters. The average oxidation rates in meteoric and Pacific waters were respectively 24.4% and 12.6% higher than the entire survey average. Moreover, Pacific and meteoric waters hosted microbial taxa of Pacific-origin that are associated with methane oxidation, *Oleispira* (γ-proteobacteria), and *Aurantivirga* (Flavobacteria). The deeper layers were characterized by low methane concentrations and low methane oxidation rate constants (av. 0.004±0.002 d^{-1}). Sea ice covered much of the Western CAA, in the same region with high sea ice meltwater concentrations. These waters also hosted higher average methane oxidation rates (av. 0.007±0.002 d^{-1}). To the east, open coastal water coincided with methane enrichment, but low chlorophyll fluorescence and weak methane oxidation. These results suggest that methane production in ice-associated Arctic blooms may be quickly oxidized by microbes that are also found in these waters, associated with seasonal biology.

1. Introduction

Methane (CH_4) is a climate-relevant gas with an equivalent warming potential 28 times more potent than carbon dioxide over a 100-year timescale (Pachauri et al., 2014); after carbon dioxide, it is responsible for about 23% of climate change in the twentieth century. The major source of methane to the atmosphere is the anthropogenic emission arising primarily from agriculture, fossil fuel production, and use of waste disposal; the remaining 20% of methane emissions come from minor sources such as wildfire, biomass burning, permafrost, termites, dams, and the ocean (Saunois et al., 2020). In the Arctic region methane concentrations are 8–10% higher than the global average, with 1890 ppb, where ppb is used to abbreviate nmol mol^{-1}, dry air mole fraction (Saunois et al., 2020; Oh et al., 2020). High concentrations of dissolved

https://doi.org/10.5194/egusphere-2023-74
Preprint. Discussion started: 6 February 2023

CH_4 in the subarctic and Arctic shelf areas were measured in recent studies (Ferré et al., 2020), however other studies showed a limited gas exchange at the air-sea interface (e.g., Fisher et al., 2011).

Understanding the role of the marine microbial metabolism associated with methane production and oxidation is an important factor for assessing the methane venting into the atmosphere. In the water column, microbial methane oxidation is an important sink for dissolved CH_4 over some depth ranges and at some locations (e.g., Mau et al., 2013, Uhlig et al., 2018). In an aerobic environment, obligate aerobic bacteria from the phyla *Proteobacteria* and *Verrucomicrobia* have been found to oxidize methane with oxygen as an electron acceptor (Dunfield et al., 2007; Pol et al., 2007). Traditionally, the proteobacterial methane-oxidizing bacteria (MOB) were divided into three groups, type I, II, and X MOB, mainly based on (i) the arrangement of their intracytoplasmic membranes, (ii) their pathway for carbon assimilation and (iii) their major cellular fatty acids (Hanson and Hanson, 1996). Currently, with 16S rDNA and functional gene phylogeny, these divisions still hold. The type II MOB are positioned within the Alphaproteobacteria and the type I and type X MOB form two distinct clades within the Gammaproteobacteria (http://hdl.handle.net/1854/LU-3230105; Hoefman, 2013). Methane-derived carbon is also assimilated in nonmethane-utilizing methylotrophs (non-MOB methylotrophs) or other bacteria in freshwater and temperate marine environments (Saidi-Mehrabad et al., 2013).

Environmental drivers control the methanogenesis (microbial production of methane in hypoxic or anoxic environments) and the methanotrophy (microbial aerobic oxidation of methane), by supplying suitable substrates for the metabolic processes. For example, strengthened upwelling stimulates the formation of phytoplankton blooms (Kudela et al., 2010), enhancing the production of dimethylsulfoniopropionate (DMSP) and increasing the formation of marine particles. This could trigger CH_4 production (Damm et al., 2008; Florez-Leiva et al., 2013; Dang & Lovell, 2016), despite aerobic waters, as it could be utilized as a C source in the methylotrophic methanogenesis. This phenomenon may be one version of the "marine methane paradox", which has received significant attention in recent years from the biogeochemical community, as it drives methane supersaturation in the surface waters of most of the world's oceans with respect to atmospheric concentrations (Karl et al., 2008; Sasakawa et al., 2008; Damm et al., 2015; Repeta et al., 2016; Lenhart et al., 2016). The "marine methane paradox" has been explained with three main processes shown in recent studies: (i) marine bacteria metabolize polysaccharide-Methylphosphonate (MPn) esters through the phosphorous redox pathways in phosphate-starved environments, producing CH_4 as a byproduct of P acquisition (Karl et al., 2008; Repeta et al., 2016; Sosa et al., 2020); (ii) temporary anoxic microenvironments could develop associated with marine particles, such as marine snow, biofilms, zooplankton guts, etc. (Dang & Lovell, 2016; Poehlein et al., 2017); (iii) the phytoplankton metabolite DMSP could be utilized as a C source in the methylotrophic methanogenesis, where bacteria aerobically produce methane as a by-product of methylphosphonate decomposition, enhanced by the activity of nitrogen-fixing microorganisms. The process is carried out by bacteria that slowly breakdown the polysaccharides belonging to phytoplankton, breaking pairs of carbon and phosphorus atoms (called C-P bonds) from their molecular structure. The microbes create methane, ethylene, and propylene gasses as byproducts (Karl et al., 2009; Damm et al. 2009; Florez-Leiva et al. 2013). These recent research findings emphasize the importance of biota in methane production and consumption; in fact, marine microbial communities drive many of the biogeochemical processes in the world's oceans, including the Arctic Ocean. Observations of microbial community structure can be used to identify ecosystem states, estimate biological activity rates, and better understand the mechanisms underlying changes in biogeochemical processes. Previous studies (e.g., Kitidis et al., 2010; Damm et al., 2010, Sultan et al., 2020; Manning et al., 2020, 2022) investigated the methane flux in different regions of the Arctic Ocean, inasmuch climate-

https://doi.org/10.5194/egusphere-2023-74
Preprint. Discussion started: 6 February 2023

relevant gases. In the Northwest Passage (NWP), a study on the methane budget revealed methane under-saturation attributed to meltwater, and methane over-saturation underneath multi-year sea ice (Kitidis et al., 2010), which is also supported by the multi-year observations, suggesting that riverine freshwater is not a major source of CH_4 in the CAA, at least during summer and early fall (Manning et al., 2022). Moreover, they assessed that the calculated rate of exchange of CH_4 between the ocean and the atmosphere was low, suggesting that this region currently plays a minor role in regulating the global atmospheric concentrations of methane across the North American Arctic Ocean (Manning et al., 2020, 2022). Hence, the major CH_4 sources in the CAA remain poorly identified.

In this study, we seek to further elucidate the methane budget in the NWP, quantify seawater methane oxidation as a sink, and detect its main association with the environmental features and the biogenic control within the water column and the sea ice. These analyses are supported by thermohaline, chemical, and biological characteristics of the water masses in relation to the methane cycle. The uniqueness of this study is the provision of paired datasets of the methane budget with associated marine microbial community, macronutrient data, and physical properties of the water masses in the CAA. In the next section, we will describe the oceanography of the Canadian Arctic Archipelago, in order to understand its hydrographic regime. In section 2, we will describe the methods developed for processing and analyzing the samples. In section 3, we will show the results achieved, and we will exhibit the dissolved methane data coupled with the in-vitro experiments for the oxidation potential. We will observe this data encompassed with the microbial taxonomy occurring in the samples, and finally, in section 4, we will discuss the outcome highlighting the major sources and sinks of methane gas, and the potential hot spots of methane oxidations within the study area. The result will provide the methane biogeography within the CAA.

1.2 Study area

The study area was centered around Parry Channel, between 71 – 77 ºN, and 100 – 79 ºW (Fig. 1). From East to West, named parts of the Channel are, Lancaster Sound, Barrow Strait, and Viscount Melville Sound. This Channel connects Baffin Bay with the Beaufort Sea on their eastern and western sides, respectively.

https://doi.org/10.5194/egusphere-2023-74
Preprint. Discussion started: 6 February 2023

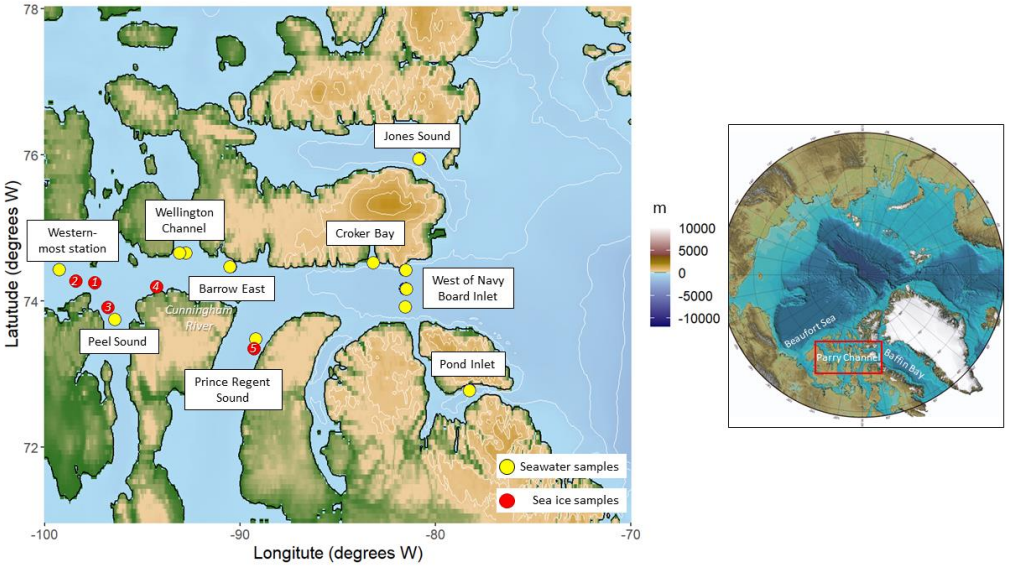

Figure 1: On the left, study area with sampling stations during the Northwest Passage cruise, July – August 2019. The yellow dots represent the water column sampling locations, whereas the red ones represent the sea ice coring sites. On the right, international bathymetric chart of the Arctic Ocean (IBCAO, Jakobsson et al., 2008), with the study area highlighted by the red rectangle.

The Arctic Ocean (AO) is characterized by a large estuarine system wherein the inputs and disposition of freshwater components provide thermohaline (buoyancy) forcing (Stigebrandt, 1984; Carmack et al., 2016). The CAA acts as a watershed discharge in the AO, as it is characterized by advection from the relatively fresh upper layers of the AO, ice melt, local river discharge, and net precipitation (Ingram and Larouche, 1987). The Northwest Passage is one of three main routes connecting the AO to the Labrador Sea and the North Atlantic (McLaughlin et al., 2007). There is a limiting sill within the Lancaster Sound located further east in Barrow Strait, where the depth is ~125 m. Continuing eastward water depths again increase gradually to ~ 500m in Lancaster Sound, then increase rapidly to over 2000 m in the center of Baffin Bay (McLaughlin et al., 2007). Flow through the CAA, from the Pacific to the Arctic to the Atlantic Oceans, is due to the higher sea level of the Pacific Ocean (McLaughlin et al., 2007). This sea level difference occurs because Pacific waters (PW) are fresher and, assuming a level of no-motion among the three ocean basins, the Arctic is thought to be 0.15 m higher than the Atlantic (Stigebrandt, 1984). During the eastward transit through Parry Channel, the PW, and Atlantic Water (AW) undergoes mixing. The shallow sill at Barrow Strait restricts the flow eastward across Lancaster Sound, constraining the deep layer of AW (McLaughlin et al., 2007). Here, the riverine runoff supplied by Cunningham River, Garnier River, and Mecham River has a big effect on the hydrodynamics and biogeochemistry of Lancaster Sound (Brown et al., 2020). The Special Report on the Ocean and Cryosphere in a Changing Climate published by the IPCC in 2021, showed how the runoff into the AO increased for Eurasian and North American rivers by 3.3 ± 1.6% and 2.0 ± 1.8% respectively (1976–2017). Another force affecting the hydrodynamics within Parry Channel is tidal energy. It enters the CAA primarily from the Atlantic Ocean and is mainly semi-diurnal. As a result, waters transiting the NWP are significantly modified by tidally-driven mixing and, in the vicinity of Barrow Strait, tidal

https://doi.org/10.5194/egusphere-2023-74
Preprint. Discussion started: 6 February 2023

currents are especially strong, reaching 50–150 cm s^{-1} (Prinsenberg and Bennetr, 1989). The water column structure is characterized by AW in the deep layers, with Pacific-origin waters overlaid, and seasonal mixed water at the top (McLaughlin et al., 2007). In the summer, the seasonal mixed layer contains fresh water from river outflow and sea-ice melt and is characterized by low salinities (24<S<31), warm temperatures, low nutrient concentrations, and high dissolved oxygen saturations. This water is the upper-most layer and its depth changes accordingly to the meltwater supply (~ 50 m in depth in Parry Channel). Below this layer is the Pacific-origin summer water. This water is characterized by relatively warm temperatures and higher salinities (31<S<32), with higher nutrient concentrations and decreasing oxygen saturations. Atlantic-origin water, within deep layers, shows maximum nutrient concentrations (McLaughlin et al., 2007). The western part of the CAA is characterized by a more consistent sea-ice coverage (Agnew and Howell, 2003). The information released by the Canadian Ice Service shows that the ranges of sea ice thickness of first-year ice in the CAA can vary from maximum values of 2.5 m in the northern and 2.0 m in the southern sections. Multi-year ice can reach a thickness of 3–5 m (Canadian Ice Service, 2002). Between freeze-up in January and break-up in late July the ice is generally immobilized as landfast ice and due to strong winds, it is also characterized by the occurrence of polynyas (Dunbar, 1969).

2. Materials and methods

The list of the sampling locations and acronyms used in this paper is the following (Fig. 1): Western-most station (WS), Wellington Channel (WC), Peel Sound (PS), Prince Regent Sound (PRS), West of Navy Board Inlet (WNBI), Crocker Bay (CB), Jones Sound (JS), Pond Inlet (PI).

2.1 Sampling procedures

Seawater and sea ice samples were collected in the vicinity of Parry Channel during the Northwest Passage Project cruise held between 17 July – 4 August 2019 onboard the Swedish icebreaker RVIB Oden. The stations include both single points and transects (see Fig. 1), covering the area with longitude 78°14.94' W - 99°16.63' W. Seawater were collected using a SeaBird 32 Water Carousel CTD rosette (24 x 12L), set with a SeaBird SBE 911+ CTD with dissolved oxygen and WETLabs Ecopuck sensors. The CTD sensor was owned and calibrated by the Swedish Polar Research Secretariat (SPRS). CTD casts and rosette bottle data are hosted at Swedish National Data Service (https://snd.gu.se/en/catalogue/study/2021-119#dataset), whereas the whole dataset and the processed CTD data are stored in Arcticdata.io (https://doi.org/10.18739/A2BN9X45M). Sea ice cores were sampled with a Kovacs ice corer drill. The sea ice concentration data was provided by the University of Bremen data archive, with 10m space resolution (seaice.uni-bremen.de, Spreen et al., 2008). Sea ice charts were collected by the Canada ice center (www.canada.ca/en/environment-climate-change/services/ice-forecasts-observations/publications/interpreting-charts).

Nutrients – A total of 239 seawater samples were collected for nutrients measurements (for processed data see: https://doi.org/10.18739/A2BN9X45M). A volume of ~ 45ml sample was filtered through 0.22-micron Millex-GP Sterile Syringe Filters with PES Membrane (Thermo Fischer Scientific) into a Corning Falcon 50 mL Conical Centrifuge Tubes (Fisher Scientific). The samples were stored onboard RVIB Oden at -20°C for post-expedition analysis.

Methane – A total of 132 (56 experimental and 76 discrete) seawater samples (Table S1) and 5 sea ice cores (Table S2) were collected and analyzed for methane concentration and isotope ratio as well as the microbial oxidation rate. The samples were both collected through multi-layer foil gas sampling bags (Restek, Bellfonte) and processed for further analysis (see details in paragraph 2.3).

https://doi.org/10.5194/egusphere-2023-74
Preprint. Discussion started: 6 February 2023

Microbial community – A total of 18 seawater samples were collected from the in-vitro methane incubations at the end of the experiments, for identifying the most abundant taxa. A cylindrical, 0.22 µm Sterivex membrane filter (Millipore Sigma, Billerica, MA) was connected to the valve of each bag for the samples collection. We removed and sealed the filters and stored them in -80 °C freezers until they were transported to the University of Rhode Island (URI), Graduate School of Oceanography (GSO) for post-expedition DNA extraction, using the DNeasy PowerWater Sterivex Kit (Qiagen, Germantown, MD) following the manufacturer's protocol (see details in paragraph 2.4).

2.2 Nutrients

Silicate, phosphate, nitrate, and nitrite concentrations were determined using a Quik Chem Series 8500 Lachat analyzer (Serial Number 061100000379 – Hach, Loveland, Colorado, USA). Heater Configuration 500 W Max, reagents and standards prepared using Quik Chem Protocols: Nitrate + Nitrite 31-107-04-1 A, Silicate 31-114-27-1 A, Phosphate 31-115-01-1 H. The analysis was carried out at the Marine Science Research Facility, URI - GSO (https://web.uri.edu/marinefacility/). To quality check the nutrients data, after excluding the data showing SD>5% between the replicated measurements, we compared nutrient data with datasets from literature (e.g., Torres-Valdés et al., 2013; Bhatia et al., 2021) and databases (e.g., DiTullio and Lee, 2019). When all the three measured nutrients (phosphate, nitrate+nitrite, silicate) showed nonagreement with the reference data, a flag = 0 was assigned to the values, highlighting outliers (D'Angelo et al., 2022 *preprint*). In total, 5 outliers were highlighted in our data frame. We also tried to identify the outliers through other procedures, but these did not show high efficacy for our dataset. In this case, calculating N:P:Si ratios for near Redfield-like consistency is likely not appropriate for our data, since denitrification plays a big part in shaping the nutrient ratios in Pacific waters, and significant freshwater inputs influence nutrients in a non-Redfield manner (Macias et al., 2019).

2.3 Methane concentration and isotope ratio measurements for discrete and experimental samples

Samples processing – Seawater for gas and isotope analysis was collected through vacuum multi-layer foil gas sampling bags equipped with a polypropylene combo valve and septum (capacity 1L and 3L, # 22950 and # 22951, Restek, Bellfonte, Pennsylvania, U.S.A.). Discrete samples were put in 3L size bags, while the experimental samples were collected in 1L size bags. Experiments were performed with approximately 0.8/0.9 L seawater, while discrete samples volumes were ~ 2.8 L. The sea ice cores were put in 3L bags and melted at room temperature for the analysis. For each sample, a headspace with hydrocarbon-free air (Airgas, Rhode Island) was made to permit multiple measurements from the same sample in a time series. For incubation samples we injected a known volume (1 to 2.5 ml, see Table 1) of gas standards with known concentration and isotopic composition (std. 1003: 2500ppmv, $\delta\,^{13}CH_4$= -66.5 ‰ Isometrics, Victoria, British Columbia, Canada). For the calibration of the instrument, we used additional methane standards.

Table 1: Information on incubation experiments. In the table are shown only the data without discrepancy between the methane oxidation rate constants of mass balance and isotope ratio.

Sample	CTD	Transect	Date	Depth (m)	CH_4 spike (ml)
22	3	Jones Sound (JS)	7/19/2019	609	1
26	3	Jones Sound (JS)	7/19/2019	7	1
36	8	West of Navy Board Inlet (WNBI)	7/23/2019	70	2.5

https://doi.org/10.5194/egusphere-2023-74
Preprint. Discussion started: 6 February 2023

37	8	West of Navy Board Inlet (WNBI)	7/23/2019	15	2.5
39	8	West of Navy Board Inlet (WNBI)	7/23/2019	15	2.5
40	8	West of Navy Board Inlet (WNBI)	7/23/2019	450	2.5
41	8	West of Navy Board Inlet (WNBI)	7/23/2019	70	2.5
43	12	West of Navy Board Inlet (WNBI)	7/24/2019	743	2.5
45	12	West of Navy Board Inlet (WNBI)	7/24/2019	401	2.5
58	21	Wellington Channel (WC)	7/26/2019	10	2.5
59	21	Wellington Channel (WC)	7/26/2019	10	2.5
76	41	Prince Regent Sound (PRS)	7/31/2019	25	2.5
78	41	Prince Regent Sound (PRS)	7/31/2019	25	2.5
79	52	Croker Bay (CB)	8/3/2019	7	2.5
81	52	Croker Bay (CB)	8/3/2019	241	2.5
82	52	Croker Bay (CB)	8/3/2019	241	2.5
83	52	Croker Bay (CB)	8/3/2019	7	2.5

The bags for in-situ measurements were stored in water at room temperature (~10°C), while the experimental bags were stored in a cold room onboard Oden at ~0ºC. Bags were analyzed for [CH_4] and isotopic signature ($\delta^{13}CH_4$) directly after preparation, following the method of Uhlig et al. (2017).

Analytic procedure – Analysis for [CH_4] and $\delta^{13}CH_4$ was performed with a Picarro G2201-i cavity ring-down spectrometer (Picarro, Santa Clara, California, U.S.A.) coupled to Small Sample Introduction Module (SSIM) (Picarro, Santa Clara, California, U.S.A.) (Uhlig and Loose, 2017). The SSIM is a sample inlet system useful for the determination of isotope ratios from discrete samples with a flow rate of approximately 22 mL min^{-1}. The SSIM further offers the possibility to dilute highly concentrated samples with hydrocarbon free zero air to reach the specification range of the analyzer of 1.8–500 ppm CH_4 (Uhlig and Loose, 2017). The dilution factor was calculated from the volume of sample (V_{sample}), volume of the dilution chamber (V_{SSIM}=22 mL), the pressure of the dilution gas (P_{SSIM}), and the atmospheric pressure (P_{atm}) recorded onboard:

$$dil\ factor\ SSIM = \frac{Pssim}{\frac{Vsample}{Vssim} * Patm}$$

To avoid water vapor, samples introduced into the SSIM passed first through a Nafion V R tube in a Permapure Gas Dryer cartridge filled with desiccant (#DM-060-24-COMP2, Permapure LLC, New Jersey, U.S.A.). Sample and standard volumes injected into the SSIM using SGE gastight syringes equipped with shutoff valves (1 mL, 5 mL and 10mL total volume - SGE, Victoria, Australia) varied between 0.01 mL and 10 mL, respectively. The SSIM coordinator software was run on fast measurement mode, syringe injection setting, and dilution with hydrocarbon-free air (Uhlig et al., 2017). The saturation capacity of the in-situ samples was calculated with the Gas-Solubility Codes in R (https://github.com/URIGSO/Gas-Solubility-Codes) and using in-situ potential temperature and practical salinity. For the sea ice, we used a salinity of 2 from the sea ice cores averaged data.

Calibration - To obtain more reproducible data, the manufacturer recommends the use of the G2201-i for methane mixing ratios >1.8 ppm (see Uhlig et al., 2017, Fig.1a). Standard gases 1001 (2500ppmv, $\delta^{13}CH_4$= -23.9 ‰), 1002 (250ppmv, $\delta^{13}CH_4$= -38.3 ‰), 1003 (2500ppmv, $\delta^{13}CH_4$= -66.5 ‰) were used to generate linear calibrations for mixing ratios and isotope ratios in order to correct for any

https://doi.org/10.5194/egusphere-2023-74
Preprint. Discussion started: 6 February 2023

transient deviations in the G2201-i analyzer, while the standard 1003 was used almost simultaneously during the measurements to calibrate the measurements via daily drift.

Estimating the oxidation rates from mass balance and isotopic fractionation – Microbial methane oxidation was determined from the methane mass balance in incubation experiments following the method of Uhlig and Loose (2017). Briefly, an aliquot of methane standard with known concentration and isotope ratio (pCH_4 = 2500 ppmv, and $\delta\,^{13}CH_4$ = -66.5 ‰) was added to every incubation to monitor the change in moles and the isotope ratio. The time of the incubations varied between 7 and 25 days, and the samples were stored in a cold bath between 0 and 1ºC.

For each methane incubation, we develop two independent measurements of the oxidation rate using the (1) molar mass balance and (2) isotopic fractionation during oxidation/production (Uhlig and Loose, 2017). During the methane microbial oxidation, the [CH_4] decreases overtime, due to the consumption made by microbes, while the isotopic signature increase as a sign of preference towards $\delta^{12}CH_4$ of microbes. The reservoir of methane (M_{tot}) here represented the sum of the mass of methane dissolved in the water (M_{gw}) and the mass of methane in the headspace (M_{ghs}) in moles.

$$M_{tot} = M_{gw} + M_{ghs}$$

As the measurements were repeated on the same sample at each time, it was important to account for the decrease in the headspace volume which affects the numbers of moles of methane that can transfer to the water for oxidation. Before calculating the oxidation rate, the total mass of CH_4 was corrected for the mass removed during sampling to obtain as in appendix A, Uhlig et al. (2017). It is routine to assume that microbial methane oxidation can be modeled as a first order kinetic process during the exponential oxidation phase (Reeburgh et al., 1991; Valentine, 2002).

$$\ln\left(\frac{Mtot_{corrected_{ti}}}{Mtot_{corrected_{t_{-1}}}}\right) = k_{ox} * t_{i_{-i-1}}$$

Where $Mtot_{corrected_{ti}}$ was calculated as:

$$Mtot_{corrected_{ti}} = Mtot_{ti} + \sum_{i=0}^{j=t_i-1} M_{sampled}$$

Therefore, the oxidation rate constant k_{ox} (with units of time^{-1}) was determined as the negative slope of the linear regression of $\ln(Mtot_{corrected})$ and the incubation time (ti). Conventionally, a positive k_{ox} indicates a decrease in methane concentration, while a negative kox indicates an increase. Molar quantities of methane in the headspace (M_{g_hs}) and water (M_{g_w}) were calculated as equilibrium concentrations according to Magen et al. (2014) with the equilibrium constant according to Yamamoto et al. (1976). In addition to the decrease in the total mass of CH_4 caused by microbial oxidation of CH_4, the carbon isotope ratio of the remaining methane pool changes due to isotopic fractionation (Whiticar, 1999). The fractionation factor $\alpha_{ox}=k_{12}/k_{13}$ (Mahieu et al., 2006) is the ratio of the kinetic constants for reactions of the heavier (k_{13}) and lighter (k_{12}) isotope CH_4 (Uhlig et al., 2017 - Appendix B). By plotting $\ln\frac{\left(\frac{1000+\delta 13CH4_{ti}}{1000+\delta\,13CH4_{t0}}\right)}{\left(\frac{1}{\alpha ox}-1\right)}$ vs. t, the first order oxidation rate constant derived from $\delta\,^{13}CH_4$ ($k_{ox.delta}$) was determined as the negative slope of the linear regression. A positive $k_{ox.delta}$ indicates an increase in $\delta\,^{13}CH_4$, and a negative $k_{ox.delta}$ a decrease. Cold marine environments with temperatures below 28ºC record fractionation factors in the range of 1.002–1.017 (Cowen et al., 2002; Grant & Whiticar, 2002; Damm et al. 2007; Fenwick et al., 2017), but for *in-situ* data it must be taken in account the mixing effects in the water column (Grant & Whiticar, 2002). As in Uhlig

https://doi.org/10.5194/egusphere-2023-74
Preprint. Discussion started: 6 February 2023

eth al. (2017), this study used α_{ox} of 1.007 as lower bounds. The microbial oxidation rates were calculated from the first order rate constant k_{ox} and the methane concentration dissolved in the water $[CH_4]_w$ during the incubation experiments as $r_{ox} = k_{ox} * [CH_4]_w$ (Uhlig et al., 2017). To validate the reproducibility of the data, we plotted the comparison of first order rate constants determined from concentration ($k_{ox,mass.balance}$) and isotope ratio ($k_{ox,isotope.ratio}$) (Fig. 2). The trend line in Figure 2 showed linear correlation of 0.52 by the Spearman's rank.

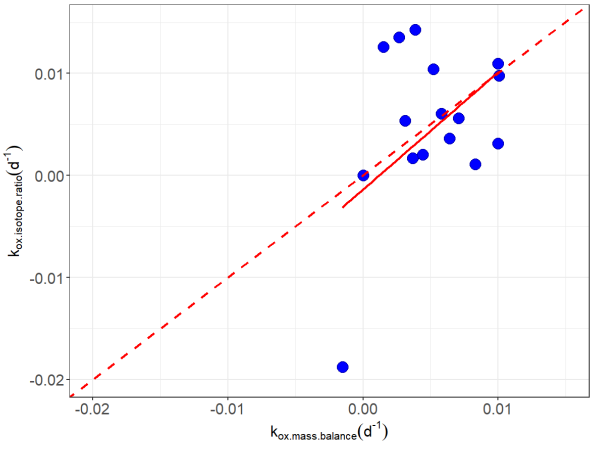

Figure 2: Comparison between first order oxidation rate constants (k_{ox}) determined from CH_4 concentration (mass balance) and isotope ratios. The red line displayed the linear model between the values (R-squared: 0.2564 p-value: 7.985e-12), whereas the red dashed line represented the 1:1 regression line.

To assess the success of the experiments and measure the microbial activity, a killed control was prepared for each sample by adding 0.1M NaOH and injecting it into the sample after the t_{final} measurement. For 1L sample, we diluted 4 g NaOH pellets in 100ml MilliQ and injected 10ml solution into the sample. The $[CH_4]$ and $\delta^{13}C\text{-}CH_4$ were measured three times within one week time frame.

Quality control - The measurements of methane concentration were not calibrated, because the standard deviation between replicate dissolved methane water samples was significantly smaller than the standard deviation in gas standards that were introduced to the Picarro analyzer, likely due to a manual artifact during syringe sampling of the gas standards. A complete calibration of $\delta^{13}CH_4$ isotope ratio was carried, because the isotope ratio was not affected in the same way as concentration during syringe sample. Linear calibration equations were determined using three standards 1003: 2500ppmv, $\delta^{13}CH_4$ = -66.5‰; 1002: 250ppmv, $\delta^{13}CH_4$= -38.3 ‰; 1001: 2500ppmv, $\delta^{13}CH_4$= -23.9 ‰; the standard 1003 was used for calculating the daily drift of the instrument. The 1003 standard revealed distinct instrumental drift while onboard the vessel Oden, as compared to the measurements on land; hence, we evaluated the dataset in two periods, from July 19th to August 4th (when the data were measured at sea), and from August 5th to August 14th (when the data were measured in the National Science Foundation facilities at Thule airbase, Greenland). For the isotope ratio, we calculated the slope and intercept of the standard 1003 overtime and used the slope and intercept from the days of full calibrations (July 19 and July 29) into the equation for the data correction.

https://doi.org/10.5194/egusphere-2023-74
Preprint. Discussion started: 6 February 2023

$$data.corrected = slope.day.cal * (data - std.1003.overtime) + (-66.5)$$

Where, -66.5 ‰ was the expected isotope ratio of the standard 1003.

Statistical criteria used to determine the oxidation rate: Duplicate in-vitro bag samples were collected for every in-vitro determination of methane concentration. This gives a matrix of 2 bags x 2 independent measurements (mass balance and isotopic fractionation) to make a robust determination of methane oxidation. The criteria that were used for this determination were as follows:

1. For each in-vitro bag, the slope in molar mass and isotope ratio, described above was subjected to a significance test using the Student's T distribution, to ensure that the slope or the rate of change in $[CH_4]$ or $\delta\,^{13}CH_4$ vs. time (oxidation or production rate) was unique from zero, within error. The number of independent measurements for each incubation was less than 15 (N<15), and we chose a confidence interval of 0.95.
2. Next, we compared the isotope ratio and molar mass determination between both bags, for quality check. First, we picked the bags showing agreement between the isotope ratio and the molar mass oxidation constants ($k_{ox.mass.balance}$ and $k_{ox.isotope.ratio}$ showing same sign). The samples showing discrepancy within the $k_{ox,mass.balance}$ and $k_{ox,isotope.ratio}$ were flagged with "0" in the final dataset (N= 37 over N_{tot}=56) and they were not considered in this manuscript.
3. Once selected the sub-dataset, we removed data showing discrepancies within the null hypothesis (for example, for the same sample we had $k_{ox.mass.balance}$ accepting and $k_{ox.isotope.ratio}$ rejecting the null hypothesis). In some cases, the whole matrix 2x2 did not show the same outcome, and we selected only data showing at least 3 agreements over 4 (2 x mass balance and 1 x isotope ratio, or vice versa).
4. The full analyses were performed with the software package R version 4.1.2 in RStudio Version 1.2.5033. Plots were prepared with base and ggplot2 packages.

Using these criteria, we can determine a definitive rate of methane oxidation vs. no measurable rate of methane oxidation. We consider a rate of 'no detectable oxidation' to also be a scientifically useful outcome because it provides a census and biogeography for where and how frequently microbial oxidation is taking place. A third outcome of the incubations can be methane production. Our experiments are not well set up to measure this as we add methane of a known isotope ratio, which might overwhelm methane produced by microbes. Nevertheless, some samples revealed methane production although all did not pass the statistical criteria described above.

2.4 DNA extraction and sequencing

Methane-oxidizing communities from seawater were analyzed for their entire community diversity (16S rRNA gene sequencing) from methane incubated samples at time 'Final' of the experiment (Uhlig et al., 2018). DNA was extracted with the PowerWater® DNA extraction kit (MoBio, Carlsbad, California, USA). The DNeasy PowerWater Sterivex Kit was used to isolate genomic DNA from Sterivex filter units (Millipore® cat. no. SVGPL10RC) without the need for enzymes or hazardous organic chemicals. Inhibitor Removal Technology® (IRT) was included to provide high-quality DNA from all types of water samples, even those containing heavy amounts of contaminants. In addition, MB Spin Columns and tube extenders allowed for one-step addition of the entire sample lysate (4.5 ml) and elution in a 50–100 µl volume. The DNeasy PowerWater Sterivex Kit protocol started with the addition and incubation of the Sterivex units with a novel filter membrane treatment. Lysis buffer was added to the units, which were then mixed. The lysate was then removed for additional mechanical lysis in a 5 ml bead beating tube. After the protein and inhibitor removal steps, extracted genetic material was captured on an MB Spin Column under vacuum.

https://doi.org/10.5194/egusphere-2023-74
Preprint. Discussion started: 6 February 2023

The column was washed, and high-quality DNA was eluted from the MB Spin Column filter membrane for use in downstream applications, including PCR and qPCR.

PCR amplicon construction and sequencing - From each extract, the V4-V5 hypervariable region of the 16S rRNA gene were amplified using forward and reverse primers from Parada et al., 2016. A 20-µl PCR reaction was performed for each sample which contained a mixture of 0.4 µl Platinum SuperFi II DNA Polymerase (Invitrogen, Carlsbad, CA), 4 µl SuperFi II Buffer (5x), 0.2 mM dNTPs, 0.5 µM of each primer, and 0.1 µl Bovine Serum Albumin (Thermo Scientific, Carlsbad, CA). We amplified each water sample in a single PCR reaction with 5 µl of DNA template. To account for possible PCR reagent contamination during PCR amplification, three samples were amplified (one for each batch of polymerase used), each one containing only laboratory water and no extract. Additionally, we completed the full DNeasy PowerWater Sterivex protocol using a sterile Sterivex filter for each kit to account for possible kit contamination. The thermal cycler program for all reactions began with an initial denaturation temperature of 98°C for 30 seconds followed by 35 cycles of 98°C for 10 seconds, 60°C for 10 seconds, and 72°C for 15 seconds, followed by a final extension of 72°C for 5 minutes. We cleaned all the samples using the Agencourt AMPure PCR Purification Kit (Beckman Coulter Life Sciences, Indianapolis, IN). Finally, all samples were sent to the University of Rhode Island Genomics and Sequencing Center and sequenced on an Illumina MiSeq platform using the Illumina MiSeq V3 chemistry at 2 x 300 cycles (NCBI BioProject PRJNA718862).

2.5 Water mass detection

Water masses were defined by a linear mixing model, the multiparameter analysis (Tomczak,1981). The contribution of each Source Water Masses (SWM, fi) was estimated for each measured point using an ordinary least squares method. The obtained fi values are in the range 0–1 and refer to the amount of a certain SWM ‘‘i’’ that is implicated in the mixing processes (Pardo et al., 2012; Newton et al., 2013). The SWMs in our study were: Atlantic Water (AW), Pacific Water (PW), Meteoric Water (MW) and Sea Ice Meltwater (SIM). We applied SA, δ18O, and an N:P-based tracer (ANP) to calculate the fractions of each sample. The endmembers were chosen according to our dataset and previous literature: for salinity, we used both extreme values (for AW and PW) and values from the literature for MW and SIM (Whitmore et al., 2020; Newton et al., 2013; Ekwurz et al., 2001); for ANP we followed Newton et al., (2013); finally, for $\delta^{18}O$ we used the extreme values for AW and PW, MW= -20 (Whitmore et al., 2020), and SIM= surface values per CTD + 2.6 ‰ (as in Newton et al., 2013).

$$f_{AW}+f_{PW}+f_{MW}+f_{SIM}=1$$

$$f_{AW}(SA)+f_{PW}(SA)+f_{MW}(SA)+f_{SIM}(SA)=SA_{obs}$$

$$f_{AW}\,(ANP)+f_{PW}\,(ANP)+f_{MW}\,(ANP)+f_{SIM}\,(ANP)=ANP_{obs}$$

$$f_{AW}(\delta^{18}O)+f_{PW}(\delta^{18}O)+f_{MW}(\delta^{18}O)+f_{SIM}(\delta^{18}O)=\delta^{18}O_{obs}$$

A more detailed description of the method can be found in D’Angelo et al., 2022 *preprint* (https://doi.org/10.5194/essd-2022-306).

3. Results

3.1 Nutrients

https://doi.org/10.5194/egusphere-2023-74
Preprint. Discussion started: 6 February 2023

Phosphate, silicate and nitrate + nitrite concentrations were measured within the water column for each site. In Fig. 3, the complete vertical profiles are displayed for each nutrient, along the longitudinal transect. The spatial scale highlighted the Pacific-origin waters containing elevated nutrients (blueish).

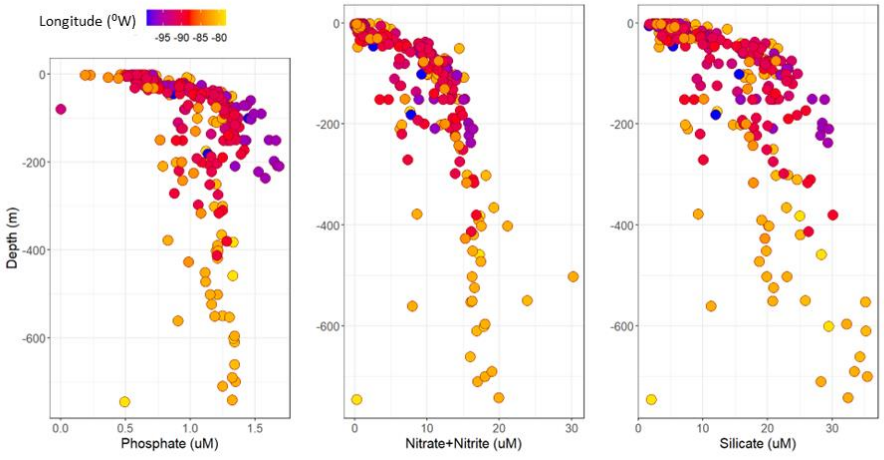

Figure 3: Phosphate, nitrate + nitrite, silicate concentrations (µM) along the CAA water column. The vertical profiles are colored by longitude of the data sites, with the most negative longitudes reflecting the western-most stations of the NWP expedition, furthest from Baffin Bay and the North Atlantic.

The concentrations range from 0 to 1.7 µM for phosphate, 1.7 to 35.4 µM for silicate and 0 to 30 µM for nitrate + nitrite. Overall, nitrate+nitrite and silicate concentrations exhibit a monotonic increase with water depthwith the exception of phosphate that had concentration maxima around 200m depth in PWs of the westernmost stations (~95 ºW, purplish in the color scale of Fig. 3). Nitrate+nitrite and silicate exhibited highest concentrations within deeper AW layers, especially toward the east (~80-85 ºW, yellowish in the color scale of Fig. 3).

3.2 Dissolved methane and isotope ratio profiles within the water column.

The seawater equilibrium supersaturation of methane in the CAA, relative to the atmospheric methane concentrations 3.42±0.05 nM, varied across space and time due to variability in temperature and salinity. The surface waters (surface to ~40 m) of the CAA mostly exceeded equilibrium saturation of CH_4, up to a maximum of 362%, while in the deeper layers methane saturation anomaly was <~100% (Fig. 4). According to the color scale in Figure 4, the methane enrichment and depletion across a longitudinal scale did not show a clear trend.

https://doi.org/10.5194/egusphere-2023-74
Preprint. Discussion started: 6 February 2023

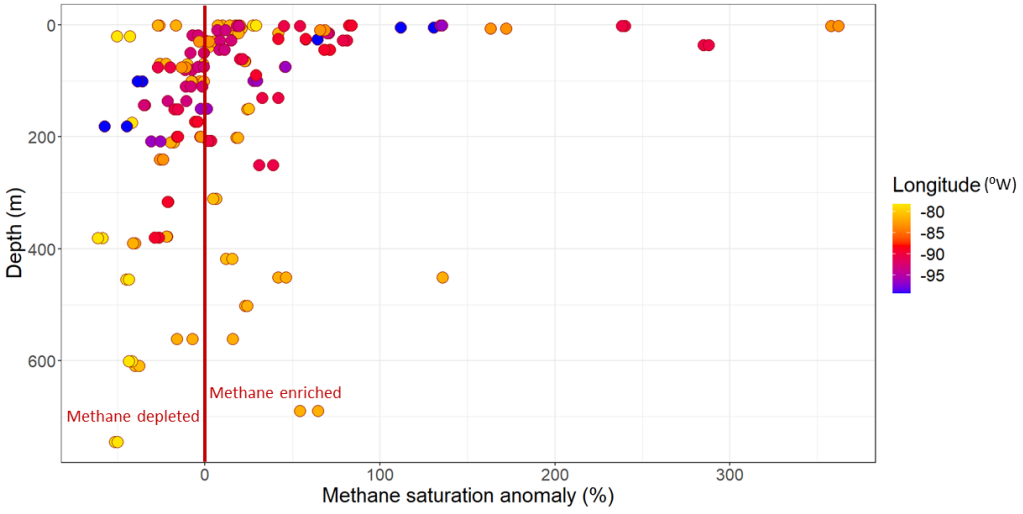

Figure 4: Methane saturation anomaly vertical profile, colored by longitude. The saturation anomaly was calculated as ($[CH_4]_{in\text{-}situ}$ / $[CH_4]_{equilibrium}$ – 1) *100, considering the solubility of the atmospheric methane at in-situ marine T and S. The dark red line indicated the methane concentrations at the equilibrium with the atmospheric methane concentration.

The weak negative correlation between CH_4 and salinity (Fig. S1) suggests that freshwater is associated with higher $[CH_4]$, but this may be a result of both salinity and CH_4 negatively covarying with depth. Figures 5 a and b show the discrete methane profiles of isotope ratio (a) and concentration coupled with the methane concentration at the atmospheric equilibrium (b) in Croker Bay. Croker Bay represented the site with the highest supply of meltwater (mainly meteoric origin, MW) and recorded the highest methane concentration (Fig. 5b, ~17nM) coupled to the lowest isotopic signature (Fig. 5a, ~-64.3 ‰). The very depleted isotopic signature could be a result of subglacial methanogenesis (Pain et al., 2020). In Croker Bay, the subsurface $[CH_4]$ was close to atmospheric equilibrium, while concentrations were higher in the upper 25 m (Fig. 5b).

https://doi.org/10.5194/egusphere-2023-74
Preprint. Discussion started: 6 February 2023

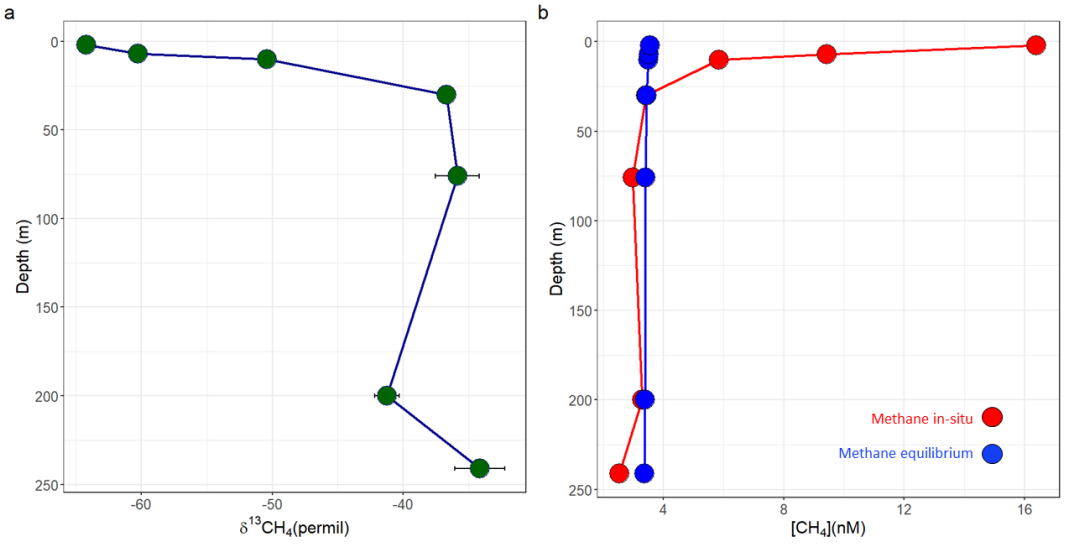

Figure 5: Methane data from samples collected in Croker Bay. a) methane isotope ratio profile; b) dissolved methane profile along the column water (methane in-situ) and methane concentration at the equilibrium relative to the atmosphere capacity (methane equilibrium).

Overall, the range of methane concentrations values varied between 2 and 17 nM across the entire dataset, whereas the isotope ratio varied between -64.2 and -17 ‰, with lowest isotope ratios in the surface ocean. The average of the [CH_4] was 4.17 ± 2.5 nM, and the values below the average were recorded within deeper layers (av. depth = 190m). West of Navy Board Inlet was the only site showing deep water methane enrichment, with ~3 nM higher concentrations in deeper layers. At this site, we recorded high turbidity within deep layers, possibly suggesting methane released from sediments (Damm et al.,2005; Graves et al., 2015; Silyakova et al., 2020). Overall, the entire data set, there is an inverse correlation (R^2: 0.35, slope = -0.18) (Figure 6) between methane concentration and isotope ratio, which is consistent with methane-associated microbial metabolism acting as the primary mechanism driving the oceanic methane budget (Hanson and Hanson, 1996), where the oxidation of methane results in a decrease of the [CH_4] and an enrichment of the heavier isotope ($\delta^{13}CH_4$). At the low range of concentrations, the variability in $\delta^{13}CH_4$ becomes quite large, suggesting the potential for a variety of inputs or sources to surface values that are near the limit of equilibrium with the atmosphere. The highest methane concentrations with lighter (more negative) isotopic signature were recorded within fresher waters, as shown by the color scale in Fig. 6.

https://doi.org/10.5194/egusphere-2023-74
Preprint. Discussion started: 6 February 2023

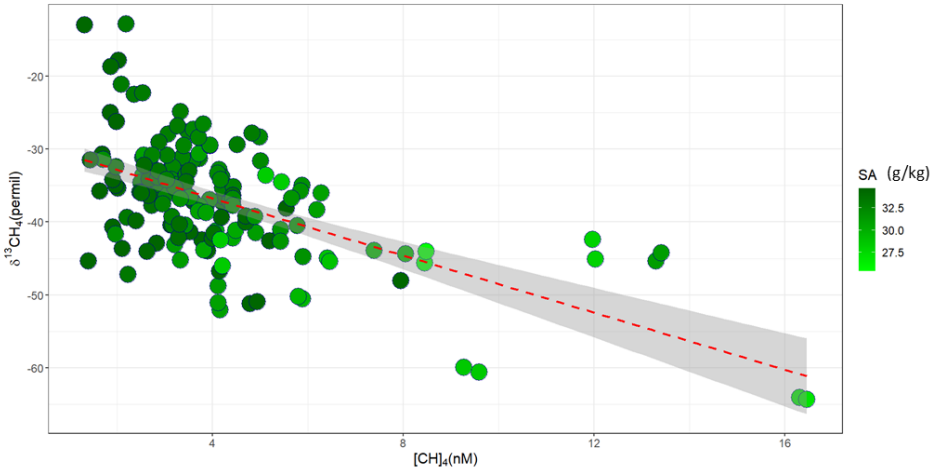

Figure 6: Relationship between the in-situ methane concentrations and the $\delta^{13}C$ isotopic ratio. The red dashed line represents the linear regression (R^2: 0.35). The color scale for the symbols show absolute salinity (SA in g/kg). A shift to higher $\delta^{13}CH_4$ coupled to a decrease in $[CH_4]$ indicates potential microbial oxidation.

3.3 Experimental methane oxidation and production

The microbial oxidation rates (r_{ox}) with rate constants (k_{ox}) were calculated as in Uhlig and Loose (2017), and the values are showed in Table 2.

Table 2: Methane oxidation rate constant (k_{ox}.av (d^{-1})) averaged between the $k_{ox.mass.balance}$ and $k_{ox.isotope.ratio}$, and the microbial methane oxidation rates (r_{ox} (nM/d)). In the table we also show the sample ID, the location (Transect) and the depth of the sample collected; moreover, we show the standard deviation between the averaged k_{ox} (kox.SD). Make the labels in the text consistent with the table.

Sample.ID	Transect	Depth	k_{ox}.av (d^{-1})	k_{ox}.SD	r_{ox} (nM/d)
22	JS	609	0.005	0.005	0.997
26	JS	7	0.003	0.001	0.458
36	WNBI	70	0.007	0.005	4.040
37	WNBI	15	0.005	0.002	2.210
39	WNBI	15	0.006	0.000	1.890
40	WNBI	450	0.006	0.001	2.700
41	WNBI	70	0.004	0.002	1.030
43	WNBI	743	0.003	0.002	1.530
45	WNBI	401	0.000	0.000	0.000
58	WC	10	0.010	0.000	3.530
59	WC	10	0.008	0.004	1.690
76	PRS	25	0.000	0.000	0.000

https://doi.org/10.5194/egusphere-2023-74
Preprint. Discussion started: 6 February 2023

78	PRS	25	0.000	0.000	0.000
79	CB	7	0.010	0.001	3.830
81	CB	241	0.009	0.007	1.090
82	CB	241	0.007	0.008	0.436
83	CB	7	0.008	0.008	0.605

Figure 7 shows the vertical distribution of the averaged methane oxidation rate constants ($k_{ox.mass.balance}$ and $k_{ox.isotope.ratio}$). The vertical trend of the methane oxidation rates showed widespread oxidation potential for methane, with higher values within the shallower waters ($k_{ox.av}$ = 0.01 d^{-1} in WC and CB ~10m depth), followed by $k_{ox.av}$ = 0.009 d^{-1} at 241 m depth in Croker. Both the oxidation rate constants ($k_{ox.mass.balance}$ and $k_{ox.isotope.ratio}$) fell in the range of values between 0 and 0.01 d^{-1}. Positive values of $k_{ox.mass.balance}$ and $k_{ox.isotope.ratio}$ indicated a decrease in methane concentrations and an enrichment of ^{13}C; conversely, negative values indicated methane production.

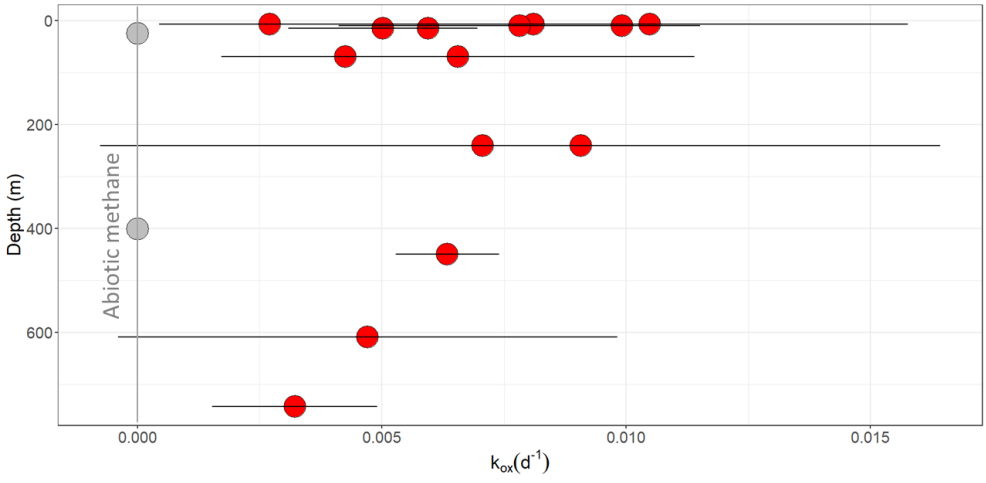

Figure 7: Vertical profiles of averaged methane oxidation rates constants for mass balance and isotope ratio. The grey dot indicates the samples showing abiotic methane, while the line at 0 determined the area with no microbial methane metabolism. The data > 0 (d^{-1}) suggested methane oxidation potential.

In summary, the waters of the CAA exhibited a net oxidative environment, in the summer of 2019. The oxidation detection limit was passed between 5 and 18 incubation days after incubation began, revealing the range of rates we observed. The samples with incubation time less than 6 days showed potential change, however, the tight range of time did not allow us to determine a factor for the detection limit.

3.4 Microbial community composition

The 16S rRNA gene analyses on the in-situ water column community revealed phylogenetic diversity. The microbial community structure of the water column was predominantly photoautotrophic, but with a high abundance of Flavobacteriaceae, *Polaribacter sp*. (Gonzalez et al., 2008) which can be heterotrophic, psychrophilic, and mesophilic. After the incubation period, the majority of the 16S rRNA gene sequences

https://doi.org/10.5194/egusphere-2023-74
Preprint. Discussion started: 6 February 2023

clustered into OTUs which were taxonomically affiliated with Alphaproteobacteria, Gammaproteobacteria and again Flavobacteriaceae (Bacteroidetes). The dominant taxa occurring in the samples showing methane oxidation were *Oleispira* (γ-proteobacteria), *Planctomarina* (α-proteobacteria), and *Aurantivirga* (flavobacteria, Song et al., 2015). Alphaproteobacteria and Gammaproteobacteria include known MOB, however, *Oleispira* and *Planctomarina* are not yet classified as such. Nevertheless, these taxa were found in Arctic methane incubations by Uhlig et al. (2018), and Gründger et al. (2021), and are therefore likely associated with methane oxidation. The Flavobacteria are known to be secondary consumers of methane, oil, or cellular decay products (Redmond & Valentine, 2012). In particular, Flavobacterium *Polaribacter sp.* is RuBisCO-lacking and the study from Alonso-Sáez et al. (2010) showed that heterotrophic CO_2 assimilation was active within the nutrient-depleted stationary phase conditions in Arctic Sea waters (DeLorenzo et al., 2012). Usually, methane oxidizers have limited ability to consume multi-carbon substrates (Hanson & Hanson, 1996), and many oil degraders have no ability to consume methane (Rojo, 2009). Flavobacteria were often associated with the degradation of high molecular weight dissolved organic carbon compounds (Cottrell and Kirchman, 2000), which may be coincidently associated with methane production (see methane paradox described above, section 1). In almost all the incubations there was occurrence of Chloroplast genome. Summarizing, our dataset emphasized the occurrence of Chloroplast genome, *Oleispira*, *Planctomarina*, and *Aurantivirga* in the methane oxidations (similar outcome of Uhlig et al., 2018 and Gründger et al., 2021). However, little is still known about this relationship, stimulating open questions on the drivers of methane oxidation activity in the Arctic Ocean.

3.5 Dissolved methane and isotope ratio in sea ice cores

Methane dissolved in sea ice stayed in the range of 3.3 and 24 nM, showing concentrations a bit higher than in seawater ([CH_4] max in CB = 17nM). The methane maxima were recorded within Westernmost Station sea ice core (24nM), however, all the samples exhibited methane oversaturation with respect to the atmospheric concentration (av. 4.7±0.01 nM) along their profiles. Core 1 at the surface and Core 2 at the bottom (Fig. 8) showed a weak deficit of methane (3.3 and 4.5 nM, respectively), whereas all other data recorded methane supersaturation with respect of atmospheric capacity. The calculation of the concentration of methane sea water at equilibrium with the normal atmosphere was derived by the Bunsen solubility coefficients, using in-situ potential temperature and a constant value of 2 for practical salinity. Core 1 and Core 2 were characterized by thicker multi-year ice (Canadian Ice Service), Core 2 was sampled in the proximity of the Westernmost station. Cores 3, 4, and 5 were collected respectively in Peel Sound, close to Cunningham River, and in Prince Regent Sound (see Fig.1), and they were characterized by first-year ice. In this study, we did not analyze the characteristics of the sea ice (e.g., permeability), which could be used as an indicator of the methane distribution (Verdugo et al., 2021), however, according to its physical and chemical parameters, we were able to identify the role the sea ice played on the methane cycle. Core 2 was oversaturated for methane up to 95cm (av. 6.86 ± 1.76 nM), below which showed undersaturation with respect to the methane atmospheric concentration (Fig. 8). The seawater [CH_4] profile showed similar values and similar trend, with oversaturation within the top layers and undersaturation below 75m depth. In Peel Sound the sea ice was characterized by nilas and thin first-year ice and surface water showed similar [CH_4] and $\delta^{13}CH_4$ (11 and 9 nM respectively in sea ice and seawater, and -50 ‰ in both). In Prince Regent Sound the sea ice was constituted by nilas and thick first-year ice (> 120 cm), and [CH_4] assessed the same value in both surface water and sea ice (~7nM), while the isotope ratio measured slightly higher values in the sea ice (~-50 ‰ in surface water and ~-42‰ in sea ice).

https://doi.org/10.5194/egusphere-2023-74
Preprint. Discussion started: 6 February 2023

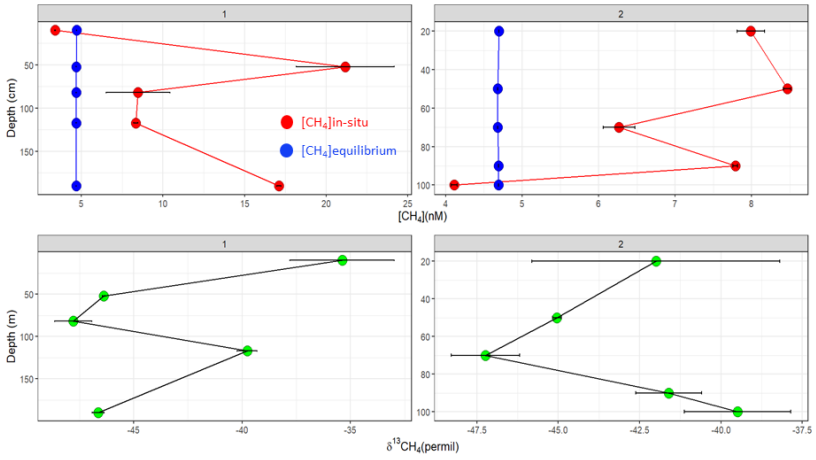

Figure 8: Methane concentrations and isotope ratios along the vertical profiles within sea ice. The red dots indicated the in-situ methane concentrations along the sea ice core, with the methane concentrations at the equilibrium relative to the atmosphere capacity (blue dots). The green dots showed the isotope ratio ($\delta^{13}CH_4$) of cores 1 and 2. The headers displayed the core numbers.

Summarizing, the $\delta^{13}C$ isotopic signature in ice cores was between -52 and -33 ‰, showing shorter variability in comparison to the in-situ water samples data.

4. Discussion

In the Canadian Arctic Archipelago waters, the dissolved methane showed a vertical stratification with methane excess mostly recorded in shallow waters. Here, we also recorded higher methane microbial oxidation rates, likely associated with Pacific-origin microbes and with the seasonal biology. Observing these results in a hydrographic contest, will elucidate about the major drivers of the methane metabolism in this specific region of the Arctic, during the summer.

4.1 The methane oxidation rates across the CAA.

The average value of the oxidation rate constant from this study was 0.005±0.003 d^{-1}. Overall, the range of values of k_{ox} and r_{ox} (describing the activity of methane-oxidizing microorganisms, Tab. 2) mainly stayed within the range of values from previous Arctic research (Mau et al., 2017; Uhlig and Loose, 2017). Moreover, the values of r_{ox} showed good fit with global methane data within a broader context (Fig. S2). The only methane oxidations data available from the CAA waters dated back to 2005 (Kitidis et al., 2010) and showed significantly higher k_{ox} values than any other measurements in the Arctic, including near seeps, k_{ox} averaged in Kitidis et al. (2010) is 0.912 d^{-1}. We note that the two oxidation rate measurements of Kitidis et al., were made using methane mass balance alone, which can be subject to high oxidation rate aberrations if methane gas leaks from the incubation chamber.

Previous studies from the Arctic and cold seeps from continental slopes across the globe (Mau et al. 2013; Boetius & Wenzhöfer, 2013) reported elevated methane oxidation activity in marine environments, coincident with high CH_4 concentrations, suggesting that MOB may be able to rapidly increase oxidation rates in response to the food source abundance. However recent studies developed in proximity of methane

https://doi.org/10.5194/egusphere-2023-74
Preprint. Discussion started: 6 February 2023

sources, such as the Arctic shelf gas seeps (Steinle et al. 2015, 2017; Gründger et al., 2021) showed that methane oxidation rates are sometimes mitigated by the seasonal variations of the hydrographical regimes, which trigger a system-wide switch of the efficiency of water column methane oxidizers. In our study, we detected higher microbial methane oxidation rates within the upper 200 m depth (see Fig.7), mainly distributed in shallow waters, with high methane concentrations (Fig. 9). The data measured in CB heavily influences the regression line trend in Figure 10 (R^2: 0.03, p-value: 0.34), as it recorded the highest value of dissolved [CH_4] coupled with high methane oxidation rates. Our results overall corroborated the thesis that methane oxidation is related to methane concentrations. We acknowledge the low amount of data available for coupled in-situ and experimental samples; however, the spatial coverage of these data is presently the best-available record of methane metabolism in the CAA waters.

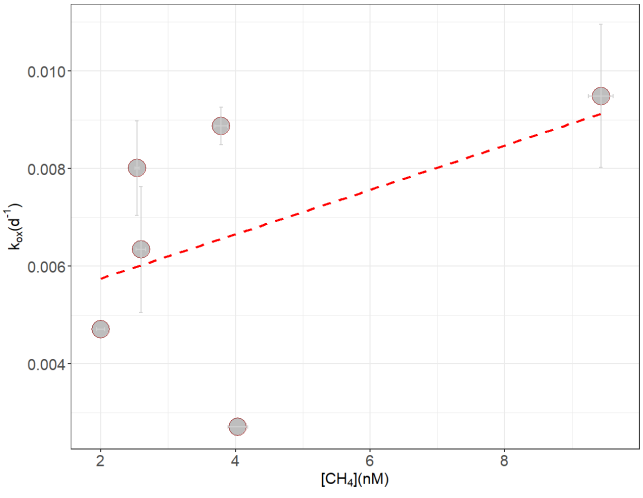

Figure 9: Methane dissolved in the water column against the averaged methane oxidation rate constants (k_{ox}). The red dashed line indicated the linear regression between the data R^2: 0.03, p-value: 0.34). The labels over the dots indicate the stations (Croker Bay, Wellington Channel, West Navy Board Inlet, Jones Sound).

To have a wider overview of the relationship between methane concentrations and oxidations, in Figure 10 we have aggregated in-situ methane and methane oxidation rate constants from several studies in both enriched and depleted methane environments (including this one). We have plotted the study-average of dissolved methane (in $\log_{10}$ scale) and its oxidation rate constant. These include data from the Gulf of Mexico (GoM), collected directly after the DWH oil spill in 2010 (Kessler et al., 2011; Rogener et al., 2018). As expected, dissolved methane in Gulf of Mexico waters was higher than Arctic waters, however, the methane oxidation rate constant was only slightly higher than the Arctic data. The methane oxidation rate constants do not appear to scale proportionately with the dissolved concentrations. Instead, the plot displayed relatively high [CH_4] associated to low k_{ox} and vice versa. This was also confirmed by the Michaelis-Menten kinetics (Button, 2010; Michaelis–Menten, 1913) (Fig. 10 right box). The result highlights that the kinetics increased hyperbolically with substrate concentration but leveled off once the

https://doi.org/10.5194/egusphere-2023-74
Preprint. Discussion started: 6 February 2023

metabolic pathway was saturated with substrate, the maximum rate achieved by the system was recorded on a value of ~20 nM [CH_4]. The Michaelis-Menten curve was generated excluding the GoM and Kitidis data, because the high values did not allow the convergence. Overall, our values of $k_{ox.}$ were in the low range of Arctic literature values, with an average of 0.006±0.002 d^{-1} (Fig. 10) and showed a great difference in magnitude with the only comparison in the same study area (Kitidis et al., 2010 with averaged k_{ox} of 0.9 d^{-1}). Conversely, the dissolved methane concentrations showed close values to Kitidis et al. (2010). The differences in the oxidation rate constant may be due to, a) the nature of the samples (melt-pond and under-ice waters, while we analyzed the entire water column), b) the number of the samples incubated for methane oxidation rates (2 in total, while we had 60 incubations), c) the method used to assess the microbial methane oxidation rate (using exclusively the mass balance, while we also analyzed the isotopic ratio and verified the bags against leaks), d) the changes to the CAA that have taken place between the expeditions (2005 vs 2019). Kitidis k_{ox} value was even higher than the values measured in the Gulf of Mexico waters after the Deepwater Horizon (DWH) oil spill in April 2010 (Kessler et al., 2011; Rogener et al., 2018) (see Fig. 10).

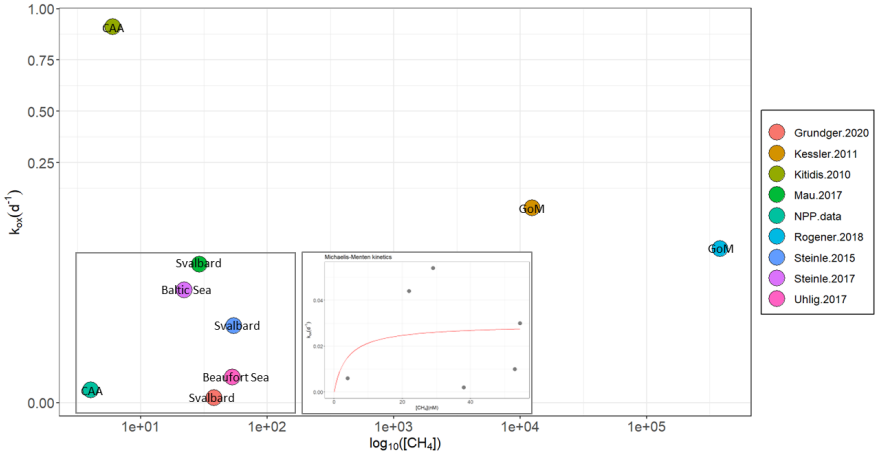

Figure 10: Averaged methane concentrations (in log_{10} scale) and oxidation rate constant from literature. In the figure, we show methane data (both in-situ and oxidation rate constant) from six studies conducted in the Arctic waters, one in the Baltic Sea, and two in the Gulf of Mexico (GoM) waters, after the Deepwater Horizon oil spill in 2010. The labels on the dots indicate the study areas. Kessler et al. (2011) show the values of k_{ox} recorded right after the Deepwater Horizon oil spill in 2010 (Apr–Sept), while the data showed by Rogener et al. (2018) account for k_{ox} values measured from May 2010 to June 2015. Steinle et al. (2015) show methane data from a cold-seep system influenced by gas hydrates along the Svalbard continental margin, in August 2011 and 2012; whereas Steinle et al. (2017) investigated the methane concentrations and oxidations in seasonally hypoxic environments (Eckernförde Bay in the SW Baltic Sea), between October 2012 and September 2014. Grundger et al. (2020) measured dissolved methane and its oxidation rate constants at the shallow shelf of Prins Karls Forlan (Arctic shelf) in the Spring and Summer between 2015 and 2017. Mau et al. (2013) show methane data from a seepage area of Svalbard, extending from 74° to 79°N. Uhlig et al (2018) show methane data from the Beaufort Sea; and finally, Kitidis et al (2010) and the NPP data are data measured from the CAA waters. Mau et al. (2017), Steinle et al. (2017), Grundger et al. (2020), Rogener et al. (2018), and Kessler et al. (2011) measured methane oxidation rates derived from

https://doi.org/10.5194/egusphere-2023-74
Preprint. Discussion started: 6 February 2023

tracer incubations using ^{3}H-CH_4. Our study and Uhlig et at (2018) used stable isotopes instead and measured both methane concentrations and isotope ratio. The x and y axis are expressed in log_{10} scale, in order to scale the different values. The grey boxes highlight the data following the Michaelis-Menten kinetics (plot window on the right).

4.2 Methane oxidation rates in oversaturated waters.

The methane oversaturation in seawater, with respect to the atmospheric concentrations, recorded the highest magnitudes in shallow Crocker Bay (17.7nM), Barrow East (14.4 nM), and Peel Sound (9.13 nM) waters, two of the three stations were located in the western part of the transect (with longitudes > 90 ºW). Croker Bay, despite being located at 83 ºW, was non-representative of the eastern Channel, because of its influence from the Devon Ice Cap drainage (D'Angelo et al., 2022). Barrow East and Peel Sound waters were characterized respectively by high watershed supply provided by Cunningham and Garnier Rivers (corroborated by McLaughlin et al., 2014), and by the watershed drainage of the marine-terminating rivers from the southern CAA (Brown et al., 2020). All three sites were characterized by high meltwater input (with MW and SIM > 10%) and detrital organic matter supply, supporting high rates of biological productivity (chlorophyll-α fluorescence and nutrients data: https://doi.org/10.18739/A2BN9X45M). Methanogenesis in the terrestrial fluvial systems and beneath terrestrial glaciers could explain the high marine CH_4 concentrations observed at these sites (Bange et al., 2010; Valentine, 2011). The isotopic signature of methane in shallow Croker Bay waters reached values < - 64 ‰ (very depleted in $\delta^{13}C$), suggesting subglacial methanogenesis (Pain et al., 2020) from the Devon Ice Cap runoff. We did not have incubation results from Barrow East and Peel Sound; however, we recorded methane oxidation potential in Croker Bay. In this site, the incubation results showed microbial methane oxidation potential in both surface and deeper layers (av. k_{ox} at surface = 0.009 ± 0.002 d^{-1}, av. k_{ox} at 241m depth = 0.008±0.001 d^{-1}, see Fig.10), suggesting that the methane dissolved in the water column could be oxidized before reaching the atmosphere.

4.3 Hydrography influencing the methane budget

To have additional insights into the role of the meltwater influencing the biogeochemistry in waters proximate to meltwater runoff, we observed the linearity between the methane data (both in-situ and ex-situ) and the freshwaters (Fig. 11). Overall, methane oxidation rates showed direct correlation with freshwater masses, suggesting the influence of the CAA meltwater runoff on the methane metabolism. This correlation does not include data CB, due to an artifact of the $\delta^{18}O$ interpolation in the MP, see D'Angelo et al, (2022) (https://doi.org/10.5194/essd-2022-306), where we recorded the highest freshwater signal for oxygen isotopes, triggered by the glacial runoff of Devon Ice Cap; hence, slightly stronger correlations between the methane data and the MW are expected. This outcome is somewhat at odds with a previous study conducted in the CAA (i.e., Manning et al., 2022), which showed that rivers (included in what we define meteoric waters) were not a significant source of CH_4 to the Arctic Ocean from early July to mid-October in years 2015-2018. Here, we did not measure the CH4 concentration within the riverine systems, so we cannot compute the flux. Nevertheless, we observe a consistent positive correlation between marine [CH4] and freshwater distribution. This discrepancy motivates future field campaigns in the Canadian Arctic Archipelago, with high spatial and temporal resolution mapping immediately before, during and after ice melt.

https://doi.org/10.5194/egusphere-2023-74
Preprint. Discussion started: 6 February 2023

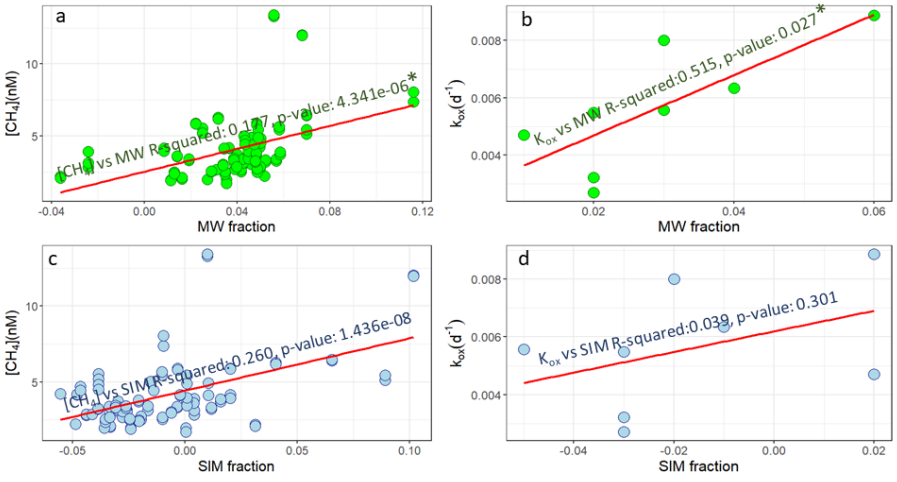

Figure 11: In-situ methane concentrations, and averaged methane oxidation rate constants (k_{ox}) in correlation with MP results. Panels (a) and (c) show methane in-situ concentrations against the meltwater masses, sea ice, and meteoric meltwaters (SIM and MW); panels (b) and (d) display the methane oxidation rate constant in relation to the meltwaters. * The results of MW potentially undergo increase, as they did not include the freshwater supply from Devon Ice Cap.

Expanding the correlations within the Pacific and Atlantic waters, dissolved methane was inversely correlated to AW (-0.4 Spearman's rank) and positively correlated with PW (0.3 Spearman's rank) (see Fig. S3). This resulted a bimodal distribution of methane across the study area (Fig. 12). Methane oxidation occurred in Pacific-dominating stations, showing an inverse correlation with AW (-0.17 Spearman's rank). In the Atlantic water regime, dissolved methane was depleted with concentrations below the equilibrium saturation range, and we recorded weaker methane microbial metabolism. The occurrence of no detectable methane oxidation in the deep layers of West Navy Board Inlet and in shallow Prince Regent Sound waters was not associated to unique thermohaline characteristics of the two sites, and unfortunately, the community structure was not analyzed in those sites.

https://doi.org/10.5194/egusphere-2023-74
Preprint. Discussion started: 6 February 2023

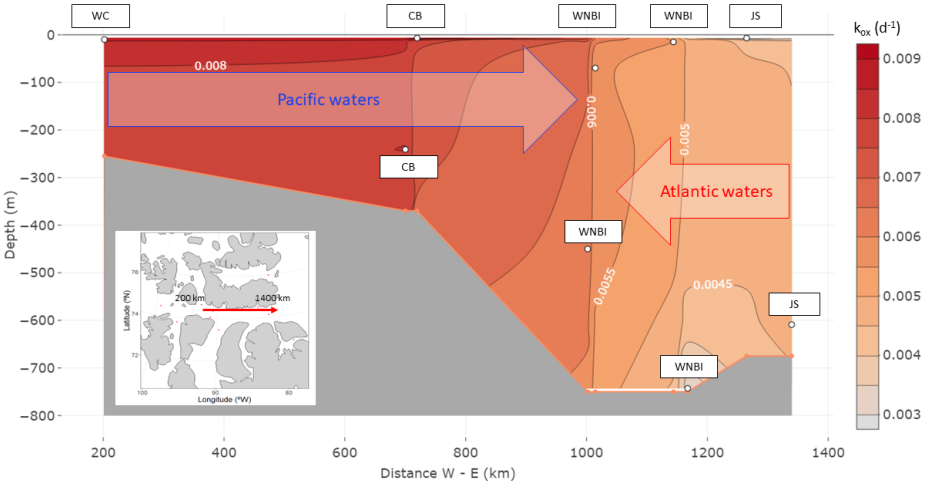

Figure 12: Section of the Parry Channel with color scale showing the k_{ox} averaged by transect and depth. Here we show the k_{ox}>0, excluding potential production signal in Western-most Station. The arrows indicate the AW and PW intruding into the channel. The white dots describe the data points, while the text boxes on top display the locations. The x axis displays the distances (in km) from the Wellington Channel 200 km (Longitude = 93.1071 ºW) to the most eastern location 1400 km (Longitude = 78.2579 ºW), see details in the map in the bottom corner.

In summary, we found weak methane metabolism in AW, while it was stronger in meltwaters and PW, with higher microbial oxidation rates and weak signal of methane potential production. These results tend to support the role of surface processes in the CAA, including meltwater and biological production as significantly associated with excess methane and higher methane oxidation, above all in the melt season (e.g., estuarine circulation). The overall picture suggested supersaturation of in-situ methane in shallow waters, coupled with faster oxidation rates in meltwater and Pacific regime, speculating prevention of the methane migration into the atmosphere towards the western CAA.

4.4 Sea Ice influence on the methane budget in the CAA.

The Western CAA contained the greatest sea ice cover, mostly as multi-year ice (MYI, see Fig. 13). Further, the satellite-derived sea ice cover and the water mass estimates of sea ice meltwater tended to coincide with greatest contributions in the West, with >10% occupying the water volume (D'Angelo et al., 2022, https://doi.org/10.5194/essd-2022-306). The fluorescence data and the phytoplanktonic community data (provided by the Menden-Deuer lab, URI-GSO), strongly indicated that on this side of the Channel there was a time lag with the Eastern Sound, showing a delay in the phytoplankton bloom. This phenomenon could have affected the methane distribution within the area, as spring blooms could activate methanotrophs and methanogens metabolism. In WS, the maximum value of dissolved methane reached 8.7nM at 5m depth, whereas the $\delta^{13}C$ isotopic ratio showed very enriched values (reaching -13 ‰ at the subsurface layers), suggesting a marine source of methane due to the preferred microbial use of ^{12}C. The microbial methane oxidation showed higher rates in the northern Sound, with the minima in ice-covered sites (Fig. 13). This result highlighted a methane-metabolic separation between the ice-covered and open-water

https://doi.org/10.5194/egusphere-2023-74
Preprint. Discussion started: 6 February 2023

Channel. Increased ice permeability at the ice bottom triggers methane release, causing low methane concentrations at the bottom of the ice and methane enrichment in the water underneath (Verdugo et al., 2021; Damm et al., 2015). This behavior was detected in the methane profile within Core 2 (collected close to the Western-most station). Here, the sea ice enriched in methane could have released the gas and the relict detritus, favoring the conditions for microbial methane production, explaining the methane deficit in the ice bottom and the methane excess in the waters underneath. The same condition, but backwards, was recorded in Core 1, where we recorded sea ice oversaturated in methane, with the top centimeters showing methane deficit. The methane initially entrapped in the sea ice was probably released into the atmosphere when the sea ice surface became permeable (Verdugo et al., 2021). Summarizing, the sea ice influenced the methane cycle in our samples, triggering the methane metabolism towards the West. Comparing our results with the ones from previous studies in the same location (Kitidis et al., 2010), sea ice similarly influenced the methane oxidation rates (SIM and k_{ox} correlation = 0.63 Spearman's rank). Our outcome, confirmed by previous studies conducted in Utqiagvik and the Central Arctic (Loose et al., 2011; Damm et al., 2015; Damm et al., 2018), suggested that the residence time of methane gas in sea ice could allow it to accumulate during the freezing period and be released during the melt period, supporting the metabolic consumption in SIM. In conclusion, we can state that the sea ice in the CAA is defined by a bimodal distribution of marine methane. In the past, other studies showed the correlation between the sea ice and the greenhouse gases in the Arctic Ocean during the summer (Damm et al., 2018, Verdugo et al., 2021), however, no data were yet referred to our study area.

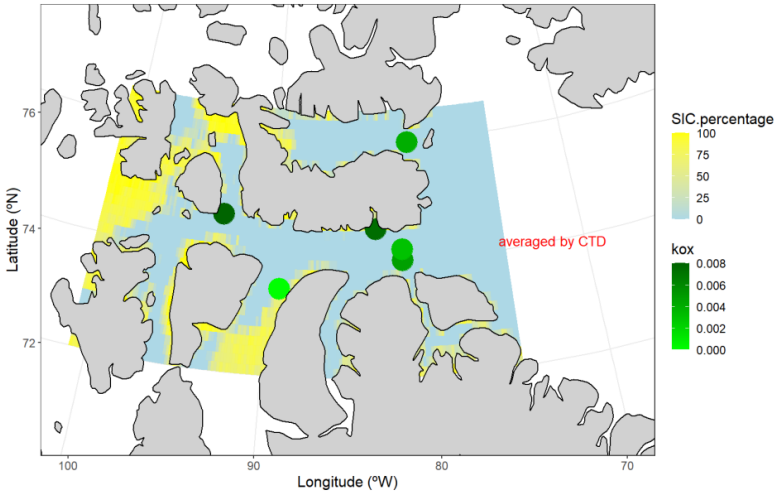

Figure 13: top view maps of the study area, with raster plots of the sea ice concentrations, and scatter plot showing $k_{ox.}$ averaged by CTD. The color scales show the SIC percentage and the k_{ox} values (d^{-1}).

4.5 Marine microbial communities driving the methane cycle in the CAA.

The genomic community composition results highlighted *Oleispira*, *Planctomarina* and *Aurantivirga* occurrence in our samples in which methane oxidation was detected, suggesting these could be the methane-

https://doi.org/10.5194/egusphere-2023-74
Preprint. Discussion started: 6 February 2023

oxidizing taxa responsible of the methane consumption in the CAA. Furthermore, the Chloroplast genome occurred in the methane-oxidated shallow samples. In Uhlig et al. (2018), *Oleispira* was also very abundant in the long-incubation samples compared to very low abundances in the in-situ samples, mainly dominated by α- and γ- proteobacteria. Here, after incubating the samples with the methane standard, the communities shifted toward higher fractions of γ-proteobacteria over time. From our analysis, we detected the shift toward α-proteobacteria instead, with *Planctomarina* dominance. The occurrence of *Oleispira* (likely belonging to *Oleispira lenta*, Wang et al., 2012) and *Aurantivirga* taxa highlighted the influence of the PW in the methane oxidation, as these taxa have been found predominantly in the North Pacific waters (Wang et al., 2012; Song et al., 2015). In particular, *Aurantivirga* occurred strictly within the bottom layer characterized by high turbidity, confirming its association with sediments. Our potential methane oxidations occurred all within waters enriched with detrital material (corroborated by the turbidity data, reaching for example 0.37 NTU in CB), supplied by the meltwater runoff. Along the water column, the Chloroplast ge. occupied the shallow layers, mainly towards the West. This confirmed the late bloom as aforementioned. This result could confirm the hypothesis of the methane production in surface waters through the P redox pathways in phosphate-starved environments (Karl et al., 2008; Repeta et al., 2016; Sosa et al., 2017 and 2020), also corroborated by the inverse correlation of -0.40 between the dissolved [CH_4] and the [$PO]_4^{3-}$ in the Spearman's rank. Concluding, the dominant taxa associated to our oxidations are not known MOB, but they have been recently connected to the methane metabolism, posing the baseline for further investigations.

5. Conclusions

Collectively, the CAA waters showed methane oversaturation with respect to atmospheric saturation capacity in the upper layers. The methane oversaturation was mainly associated with the meltwaters and primary production (in nutrient depleted environments), likely following the Methylphosphonate (MPn) esters metabolization, as explained in Repeta et al. (2016) and Sousa et al. (2020). The CAA waters were characterized by methane oxidizers, with 74% showing potential methane oxidation, 5% showing potential production, and 21% resulting methane abiotic (over 17 samples). The fastest oxidation rates were recorded within meltwaters and Pacific-origin Waters, however the k_{ox} showed lower rates than the k_{ox} measured during a cruise held in 2005 in the CAA (Kitidis et al., 2010). The community structure likely responsible for the methane oxidation was characterized by three main groups nonbelonging to known MOB, but recently associated with the methane metabolism (*Aurantivirga, Oleispira and Planktomarina*); *Aurantivirga* and *Oleispira* were both isolated from PWs. This outcome suggested that the PW predominance of the CAA waters could define hotspots for methane oxidations. The ice-covered site showed the lowest methane oxidation rates, suggesting potential methane production, likely due to the late phytoplankton bloom, delayed by the sea ice coverage. This data strengthened the hypothesis that the sea ice acted as a barrier for the gas exchange, defining the underneath water's hotspot for methane excess during the summer. The Pacific regime of the CAA was characterized by methane oxidizers predominance and exhibited high potential oxidation rates.

Summarizing, the sea ice would potentially trigger methane production, the Pacific and melt waters would enhance methanotrophy, while the Atlantic Waters would be mostly methane abiotic. We could divide the entire study area into four environments, according to the methane distribution: (a) sea ice, with methane excess; (b) meltwaters (meteoric and sea ice melt), characterized by methane oxidations in oversaturated waters; (c) Pacific waters, with high methane oxidation rates, likely due to methanotrophs; (d) Atlantic regime, mostly abiotic for methane. Due to the Atlantification of the Arctic Ocean (Polyakov et al., 2017,

https://doi.org/10.5194/egusphere-2023-74
Preprint. Discussion started: 6 February 2023

2020), we would expect higher intrusion of AW in the CAA at the expense of PW, with consequent sea ice melting. According to our outcome, the takeaway is that in such a scenario, we would expect stronger stratification, with methane excess alternated to microbial oxidations at the top 200m, overlaying methane-depleted waters, with reduced methane oxidation rates.

Data availability

The produced database of this study has been archived in Arctic Data Center and can be assessed using the following link: https://doi.org/10.18739/A2BN9X45M.

Author contribution

B.L. designed the research. B.L. and A.D. implemented the study. A.D., C.G-E., Z.K., J.S., F.C., N.V., H.R., T.E., S.U., B.L., were involved in the sampling activities. A.D., B.L., N.V., H.R., T.E., S.U., performed the analysis. A.D., B.L., A.L.K., M.G-M., F.C., C.G-E. processed the data. A.D. and B.L. wrote the manuscript, with input from all authors. The authors declare that they have no conflict of interest.

Competing interests

The authors declare that they have no conflict of interest.

Acknowledgements

We would extend our gratitude to the entire crew of the RVIB Oden, and the Swedish Polar Research Secretariat team for the logistic effort. We greatly appreciated the involvement of all the undergraduates and scientists participating in the expedition. We thank our Arctic guide Sarah Scriver for assistance. We acknowledge the local communities for their collaboration, and the Marine Science Research Facility at GSO - URI, for carrying out the nutrients analysis. We deeply thank NSF facilities at Thule airbase, Polarfield, Greenland for the help provided in Thule, Greenland. The study was supported by the National Science Foundation Awards #1748318 and # 1821900, with additional support from the Heising Simons Foundation. We gratefully acknowledge the NSF Program Officer for the Northwest Passage Project, Valentine Kass, and the lead PI of the project, Gail Scowcroft (Associate Director, Inner Space Center, University of Rhode Island).

https://doi.org/10.5194/egusphere-2023-74
Preprint. Discussion started: 6 February 2023

References

Agnew, T. and Howell, S.: The use of operational ice charts for evaluating passive microwave ice concentration data, Atmosphere - Ocean, 41, 317–331, https://doi.org/10.3137/ao.410405, 2003.

Alonso-Sáez, L., Galand, P. E., Casamayor, E. O., Pedrós-Alió, C., and Bertilsson, S.: High bicarbonate assimilation in the dark by Arctic bacteria, ISME Journal, 4, 1581–1590, https://doi.org/10.1038/ismej.2010.69, 2010.

Anthony, C. (1982) The Biochemistry of Methylotrophs. London, UK: Academic Press.

Bange, H. W., Freing, A., Kock, A., & Löscher, C. R. (2010). Marine pathways to nitrous oxide. In Nitrous Oxide and Climate Change (1st ed., pp. 36–62). Routledge. https://doi.org/10.4324/9781849775113

Bhatia, M. P., Waterman, S., Burgess, D. O., Williams, P. L., Bundy, R. M., Mellett, T., Roberts, M., and Bertrand, E. M.: Glaciers and Nutrients in the Canadian Arctic Archipelago Marine System, Global Biogeochem Cycles, 35, https://doi.org/10.1029/2021GB006976, 2021.

Boden, Rich, et al. "Novel Methylotrophic Bacteria Isolated From the River Thames (London, UK)." Environmental Microbiology, vol. 10, no. 12, 2008, pp. 3225-36.

Boetius, A. and Wenzhöfer, F.: Seafloor oxygen consumption fuelled by methane from cold seeps, https://doi.org/10.1038/ngeo1926, September 2013.

Brown, K. A., Williams, W. J., Carmack, E. C., Fiske, G., François, R., McLennan, D., and Peucker-Ehrenbrink, B.: Geochemistry of Small Canadian Arctic Rivers with Diverse Geological and Hydrological Settings, J Geophys Res Biogeosci, 125, https://doi.org/10.1029/2019JG005414, 2020.

Brusseau, G. A., Tsien, H.-C., Hanson, R. S., and Wackett, L. P.: Optimization of trichloroethylene oxidation by methanotrophs and the use of a colorimetric assay to detect soluble methane monooxygenase activity, Biodegradation, Kluwer Academic Publishers, 19–29 pp., 1990.

Carmack, E. C., Yamamoto-Kawai, M., Haine, T. W. N., Bacon, S., Bluhm, B. A., Lique, C., Melling, H., Polyakov, I. v., Straneo, F., Timmermans, M. L., and Williams, W. J.: Freshwater and its role in the Arctic Marine System: Sources, disposition, storage, export, and physical and biogeochemical consequences in the Arctic and global oceans, https://doi.org/10.1002/2015JG003140, 1 March 2016.

Chistoserdova L. Modularity of methylotrophy, revisited. Environ Microbiol. 2011 Oct;13(10):2603-22. doi: 10.1111/j.1462-2920.2011.02464.x. Epub 2011 Mar 28. PMID: 21443740.

Cottrell, M. T. and Kirchman, D. L.: Community Composition of Marine Bacterioplankton Determined by 16S rDNA Gene Clone Libraries and Fluorescence In Situ Hybridization, APPLIED AND ENVIRONMENTAL MICROBIOLOGY, 5116–5122 pp., 2000.

Cowen, J. P., Wen, X., and Popp, B. N.: PII S0016-7037(02)00975-4 Methane in aging hydrothermal plumes, 2002.

Crespo-Medina, M., Twing, K. I., Kubo, M. D. Y., Hoehler, T. M., Cardace, D., WCollom, T., and Schrenk, M. O.: Insights into environmental controls on microbial communities in a continental serpentinite aquifer using a microcosm-based approach, Front Microbiol, 5, https://doi.org/10.3389/fmicb.2014.00604, 2014.

https://doi.org/10.5194/egusphere-2023-74
Preprint. Discussion started: 6 February 2023

D'Angelo, A., Garcia-Eidell, C., Knowlton, C., Gingras, A., Morin, H., Coleman, D., Kaelblein, J., Raziuddin, H., VanKeersbilck, N., Rivera, T. J., Kopka, K., Boleaga, Y., Estes, K., Nodal, A., Schulze, E., Ewa, T., Shaban, M., Umar, S., Santana, R., Strock, J., Gruebel, E., Digilio, M., Ludkin, R., Gong, D., Kerrigan, Z., Otokiak, M., Crable, F., Trenholm, N., Millstone, T., Montenegro, K., Kim, M., Porter, G., Ketter, T., Berkelhammer, M., King, A. L., Gonzalez-Meler, M. A., and Loose, B.: Water masses distribution in the Canadian Arctic Archipelago: Implementation of the Optimal MultiParameter analysis (OMP), Earth Syst. Sci. Data Discuss. [preprint], https://doi.org/10.5194/essd-2022-306, 2022.

Damm, E., Bauch, D., Krumpen, T., Rabe, B., Korhonen, M., Vinogradova, E., and Uhlig, C.: The Transpolar Drift conveys methane from the Siberian Shelf to the central Arctic Ocean, Sci Rep, 8, https://doi.org/10.1038/s41598-018-22801-z, 2018.

Damm, E., Helmke, E., Thoms, S., Schauer, U., Nöthig, E., Bakker, K., Kiene, R. P., and Wegener, A.: Methane production in aerobic oligotrophic surface water in the central Arctic Ocean, Biogeosciences, 1099–1108 pp., 2010.

Damm, E., Kiene, R. P., Schwarz, J., Falck, E., and Dieckmann, G.: Methane cycling in Arctic shelf water and its relationship with phytoplankton biomass and DMSP, Mar Chem, 109, 45–59, https://doi.org/10.1016/j.marchem.2007.12.003, 2008.

Damm, E., Rudels, B., Schauer, U., Mau, S., and Dieckmann, G.: Methane excess in Arctic surface water-triggered by sea ice formation and melting, Sci Rep, 5, https://doi.org/10.1038/srep16179, 2015.

Dang, H. and Lovell, C. R.: Microbial Surface Colonization and Biofilm Development in Marine Environments, Microbiology and Molecular Biology Reviews, 80, 91–138, https://doi.org/10.1128/mmbr.00037-15, 2016.

DeLorenzo, S., Bräuer, S. L., Edgmont, C. A., Herfort, L., Tebo, B. M., and Zuber, P.: Ubiquitous Dissolved Inorganic Carbon Assimilation by Marine Bacteria in the Pacific Northwest Coastal Ocean as Determined by Stable Isotope Probing, PLoS One, 7, https://doi.org/10.1371/journal.pone.0046695, 2012.

DiTullio G, Lee P (2019) Dissolved nutrient concentrations, High Arctic Ocean, August-September 2018. Arctic Data Center. https://doi.org/10.18739/A2CN6Z03F

Dunbar, Moira. "The Geographical Position of the North Water." *Arctic* 22: 438-441, DOI:10.14430/ARCTIC3235 Corpus ID: 129164760, 1969.

Dunfield PF, Yuryev A, Senin P, Smirnova AV, Stott MB, Hou S, Ly B, Saw JH, Zhou Z, Ren Y, Wang J, Mountain BW, Crowe MA, Weatherby TM, Bodelier PL, Liesack W, Feng L, Wang L, Alam M. Methane oxidation by an extremely acidophilic bacterium of the phylum Verrucomicrobia. Nature. 2007 Dec 6;450(7171):879-82. doi: 10.1038/nature06411. Epub 2007 Nov 14. PMID: 18004300.

Fenwick, L., Capelle, D., Damm, E., Zimmermann, S., Williams, W. J., Vagle, S., and Tortell, P. D.: Methane and nitrous oxide distributions across the North American Arctic Ocean during summer, 2015, J Geophys Res Oceans, 122, 390–412, https://doi.org/10.1002/2016JC012493, 2017.

Ferré, B., Jansson, P. G., Moser, M., Serov, P., Portnov, A., Graves, C. A., Panieri, G., Gründger, F., Berndt, C., Lehmann, M. F., and Niemann, H.: Reduced methane seepage from Arctic sediments during cold bottom-water conditions, Nat Geosci, 13, 144–148, https://doi.org/10.1038/s41561-019-0515-3, 2020.

https://doi.org/10.5194/egusphere-2023-74
Preprint. Discussion started: 6 February 2023

902 Fisher, R. E., Sriskantharajah, S., Lowry, D., Lanoisellé, M., Fowler, C. M. R., James, R. H., Hermansen,
903 O., Lund Myhre, C., Stohl, A., Greinert, J., Nisbet-Jones, P. B. R., Mienert, J., and Nisbet, E. G.: Arctic
904 methane sources: Isotopic evidence for atmospheric inputs, Geophys Res Lett, 38,
905 https://doi.org/10.1029/2011GL049319, 2011.

906 Florez-Leiva, L., Damm, E., and Farías, L.: Methane production induced by dimethylsulfide in surface
907 water of an upwelling ecosystem, Prog Oceanogr, 112–113, 38–48,
908 https://doi.org/10.1016/j.pocean.2013.03.005, 2013.

909 Gonzalez, J.M., Fernandez-Gomez, B., Fernandez-Guerra, A., Gomez-Consarnau, L., Sanchez, O., Coll-
910 Llado, M., Del Campo, J., Escudero, L., Rodriguez-Martinez, R., Alonso-Saez, L., Latasa, M., Paulsen, I.,
911 Nedashkovskaya, O., Lekunberri, I., Pinhassi, J., and Pedros-Alio, C. "Genome analysis of the
912 proteorhodopsin-containing marine bacterium Polaribacter sp. MED152 (Flavobacteria)." Proc. Natl. Acad.
913 Sci. USA (2008) 105:8724-8729.

914 Grant, N. J. and Whiticar, M. J.: Stable carbon isotopic evidence for methane oxidation in plumes above
915 Hydrate Ridge, Cascadia Oregon Margin, Global Biogeochem Cycles, 16, 71-1-71–13,
916 https://doi.org/10.1029/2001gb001851, 2002.

917 Graves, C. A., L. Steinle, G. Rehder, H. Niemann, D. P. Connelly, D. Lowry,R. E. Fisher, A. W. Stott, H.
918 Sahling, andR. H. James (2015), Fluxes and fate ofdissolved methane released at theseafloor at the landward
919 limit of thegas hydrate stability zone offshorewestern Svalbard, J. Geophys. Res.Oceans,120, 6185–6201,
920 doi:10.1002/2015JC011084.

921 Gründger, F., Probandt, D., Knittel, K., Carrier, V., Kalenitchenko, D., Silyakova, A., Serov, P., Ferré, B.,
922 Svenning, M. M., and Niemann, H.: Seasonal shifts of microbial methane oxidation in Arctic shelf waters
923 above gas seeps, Limnol Oceanogr, 66, 1896–1914, https://doi.org/10.1002/lno.11731, 2021.

924 Hanson RS, Hanson TE. Methanotrophic bacteria. Microbiol Rev. 1996 Jun;60(2):439-71. doi:
925 10.1128/mr.60.2.439-471.1996. PMID: 8801441; PMCID: PMC239451.

926 Hoefman S. From nature to nurture: isolation, physiology and preservation of methane-oxidizing bacteria.
927 [Ghent, Belgium]: Ghent University. Faculty of Sciences; 2013.

928 Ingram, R. G. and Larouche, P.: Variability of an under-ice river plume in Hudson Bay, J Geophys Res
929 Oceans, 92, 9541–9547, https://doi.org/10.1029/JC092iC09p09541, 1987.

930 Jakobsson, M., R. Macnab, L. Mayer, R. Anderson, M. Edwards, J. Hatzky, H. W. Schenke, and P. Johnson.
931 An improved bathymetric portrayal of the Arctic Ocean: Implications for ocean modeling and geological,
932 geophysical and oceanographic analyses, Geophysical Research Letters, DOI: 10.1029/2008GL033520,
933 2008.

934 Jensen, S., Neufeld, J. D., Birkeland, N. K., Hovland, M., and Murrell, J. C.: Methane assimilation and
935 trophic interactions with marine Methylomicrobium in deep-water coral reef sediment off the coast of
936 Norway, FEMS Microbiol Ecol, 66, 320–330, https://doi.org/10.1111/j.1574-6941.2008.00575.x, 2008.

937 Karl, D., Beversdorf, L., Björkman, K. et al. Aerobic production of methane in the sea. Nature Geosci 1,
938 473–478 (2008). https://doi.org/10.1038/ngeo234

Kessler JD, Valentine DL, Redmond MC, Du M, Chan EW, Mendes SD, Quiroz EW, Villanueva CJ, Shusta SS, Werra LM, Yvon-Lewis SA, Weber TC. A persistent oxygen anomaly reveals the fate of spilled methane in the deep Gulf of Mexico. Science. 2011 Jan 21;331(6015):312-5. doi: 10.1126/science.1199697. Epub 2011 Jan 6. PMID: 21212320.

Kitidis, V., Upstill-Goddard, R. C., and Anderson, L. G.: Methane and nitrous oxide in surface water along the North-West Passage, Arctic Ocean, Mar Chem, 121, 80–86, https://doi.org/10.1016/j.marchem.2010.03.006, 2010.

Kudela, R. M., Seeyave, S., and Cochlan, W. P.: The role of nutrients in regulation and promotion of harmful algal blooms in upwelling systems, Prog Oceanogr, 85, 122–135, https://doi.org/10.1016/j.pocean.2010.02.008, 2010.

Lenhart, K., Klintzsch, T., Langer, G., Nehrke, G., Bunge, M., Schnell, S., and Keppler, F.: Evidence for methane production by the marine algae Emiliania huxleyi, Biogeosciences, 13, 3163–3174, https://doi.org/10.5194/bg-13-3163-2016, 2016.

Loose, B., Schlosser, P., Perovich, D., Ringelberg, D., Ho, D. T., Takahashi, T., Richter-Menge, J., Reynolds, C. M., Mcgillis, W. R., and Tison, J. L.: Gas diffusion through columnar laboratory sea ice: Implications for mixed-layer ventilation of CO2 in the seasonal ice zone, Tellus B Chem Phys Meteorol, 63, 23–39, https://doi.org/10.1111/j.1600-0889.2010.00506.x, 2011.

Mahieu, K., Visscher, A. de, Vanrolleghem, P. A., and Cleemput, O. van: Carbon and hydrogen isotope fractionation by microbial methane oxidation: Improved determination, in: Waste Management, 389–398, https://doi.org/10.1016/j.wasman.2005.11.006, 2006.

Mau, S., Blees, J., Helmke, E., Niemann, H., and Damm, E.: Vertical distribution of methane oxidation and methanotrophic response to elevated methane concentrations in stratified waters of the Arctic fjord Storfjorden (Svalbard, Norway), Biogeosciences, 10, 6267–6268, https://doi.org/10.5194/bg-10-6267-2013, 2013.

Mclaughlin, F., Carmack, E., Proshutinsky, A., Krishfield, R. A., Guay, C., Yamamoto-Kawai, M., Jackson, J. M., and Williams, B.: The Rapid Response of the Canada Basin to Climate Forcing: FROM BELLWETHER TO ALARM BELLS, Source: Oceanography, 24, 146–159, https://doi.org/10.2307/24861309, 2007.

Oh, Y., Zhuang, Q., Liu, L., Welp, L. R., Lau, M. C. Y., Onstott, T. C., Medvigy, D., Bruhwiler, L., Dlugokencky, E. J., Hugelius, G., D'Imperio, L., and Elberling, B.: Reduced net methane emissions due to microbial methane oxidation in a warmer Arctic, Nat Clim Chang, 10, 317–321, https://doi.org/10.1038/s41558-020-0734-z, 2020.

Pachauri, R. K., Mayer, Leo., and Intergovernmental Panel on Climate Change: Climate change 2014 : synthesis report, 151 pp., n.d.

Poehlein, A., Solano, J. D. M., Flitsch, S. K., Krabben, P., Winzer, K., Reid, S. J., Jones, D. T., Green, E., Minton, N. P., Daniel, R., and Dürre, P.: Microbial solvent formation revisited by comparative genome analysis, Biotechnol Biofuels, 10, https://doi.org/10.1186/s13068-017-0742-z, 2017.

Pol A, Heijmans K, Harhangi HR, Tedesco D, Jetten MS, Op den Camp HJ. Methanotrophy below pH 1 by a new Verrucomicrobia species. Nature. 2007 Dec 6;450(7171):874-8. doi: 10.1038/nature06222. Epub 2007 Nov 14. PMID: 18004305.

Polyakov, I. V., Alkire, M. B., Bluhm, B. A., Brown,K. A., Carmack, E. C., Chierici, M., Danielson, S. L.,Ellingsen, I., Ershova, E. A., Gårdfeldt, K., Ingvaldsen, R.B., Pnyushkov, A. V., Slagstad, D., and Wassmann, P.: Bo-realization of the Arctic Ocean in Response to AnomalousAdvection From Sub-Arctic Seas, Front. Mar. Sci., 7, 491,https://doi.org/10.3389/fmars.2020.00491, 2020.

Polyakov, I. V., Pnyushkov, A. V., Alkire, M. B., Ashik, I. M., Bau-mann, T. M., Carmack, E. C., Goszczko, I., Guthrie, J., Ivanov, V.V., Kanzow, T., Krishfield, R., Kwok, R., Sundfjord, A., Morison,J., Rember, R., and Yulin, A.: Greater role for Atlantic inflows onsea-ice loss in the Eurasian Basin of the Arctic Ocean, Science,356, 285–291, https://doi.org/10.1126/science.aai8204, 2017.

Prinsenberg, S. J. and Bennetr, E. B.: Transport between Peel Sound and Barrow Strait in the Canadian Arctic, Continental Shelf Research, 427–444 pp., 1989.

Reeburgh, W. S., Ward, B. B., Whalen, S. C., Sandbeck, K. A., Kilpatrick, K. A., and Kerkhof, L. J.: Black Sea methane geochemistry, Deep-Sea Research, Part A, 38, https://doi.org/10.1016/s0198-0149(10)80030-5, 1991.

Repeta, D. J., Ferrón, S., Sosa, O. A., Johnson, C. G., Repeta, L. D., Acker, M., Delong, E. F., and Karl, D. M.: Marine methane paradox explained by bacterial degradation of dissolved organic matter, Nat Geosci, 9, 884–887, https://doi.org/10.1038/ngeo2837, 2016.

Rogener, M. K., Bracco, A., Hunter, K. S., Saxton, M. A., and Joye, S. B.: Long-term impact of the Deepwater Horizon oil well blowout on methane oxidation dynamics in the northern Gulf of Mexico, Elementa, 6, https://doi.org/10.1525/elementa.332, 2018.

Rojo, F.: Degradation of alkanes by bacteria: Minireview, https://doi.org/10.1111/j.1462-2920.2009.01948.x, 2009.

Saidi-Mehrabad, A., He, Z., Tamas, I., Sharp, C. E., Brady, A. L., Rochman, F. F., Bodrossy, L., Abell, G. C. J., Penner, T., Dong, X., Sensen, C. W., and Dunfield, P. F.: Methanotrophic bacteria in oilsands tailings ponds of northern Alberta, ISME Journal, 7, 908–921, https://doi.org/10.1038/ismej.2012.163, 2013.

Sasakawa, M., Tsunogai, U., Kameyama, S., Nakagawa, F., Nojiri, Y., and Tsuda, A.: Carbon isotopic characterization for the origin of excess methane in subsurface seawater, J Geophys Res Oceans, 113, https://doi.org/10.1029/2007JC004217, 2008.

Saunois, M., R. Stavert, A., Poulter, B., Bousquet, P., G. Canadell, J., B. Jackson, R., A. Raymond, P., J. Dlugokencky, E., Houweling, S., K. Patra, P., Ciais, P., K. Arora, V., Bastviken, D., Bergamaschi, P., R. Blake, D., Brailsford, G., Bruhwiler, L., M. Carlson, K., Carrol, M., Castaldi, S., Chandra, N., Crevoisier, C., M. Crill, P., Covey, K., L. Curry, C., Etiope, G., Frankenberg, C., Gedney, N., I. Hegglin, M., Höglund-Isaksson, L., Hugelius, G., Ishizawa, M., Ito, A., Janssens-Maenhout, G., M. Jensen, K., Joos, F., Kleinen, T., B. Krummel, P., L. Langenfelds, R., G. Laruelle, G., Liu, L., MacHida, T., Maksyutov, S., C. McDonald, K., McNorton, J., A. Miller, P., R. Melton, J., Morino, I., Müller, J., Murguia-Flores, F., Naik, V., Niwa, Y., Noce, S., O'Doherty, S., J. Parker, R., Peng, C., Peng, S., P. Peters, G., Prigent, C., Prinn, R., Ramonet,

M., Regnier, P., J. Riley, W., A. Rosentreter, J., Segers, A., J. Simpson, I., Shi, H., J. Smith, S., Paul Steele, L., F. Thornton, B., Tian, H., Tohjima, Y., N. Tubiello, F., Tsuruta, A., Viovy, N., Voulgarakis, A., S. Weber, T., van Weele, M., R. Van Der Werf, G., F. Weiss, R., Worthy, D., Wunch, D., Yin, Y., Yoshida, Y., Zhang, W., Zhang, Z., Zhao, Y., Zheng, B., Zhu, Q., Zhu, Q., and Zhuang, Q.: The global methane budget 2000-2017, Earth Syst Sci Data, 12, 1561–1623, https://doi.org/10.5194/essd-12-1561-2020, 2020.

Silyakova, A., and others. 2020. Physical controls of dynamics of methane venting from a shallow seep area west of Svalbard. Cont. Shelf Res. 194: 104030.

Song, J., Choi, A., Im, M., Joung, Y., Yoshizawa, S., Cho, J. C., and Kogure, K.: Aurantivirga profunda gen. nov sp. nov isolated from deep-seawater, a novel member of the family flavobacteriaceae, Int J Syst Evol Microbiol, 65, 4850–4856, https://doi.org/10.1099/ijsem.0.000662, 2015.

Sosa, O. A., Burrell, T. J., Wilson, S. T., Foreman, R. K., Karl, D. M., and Repeta, D. J.: Phosphonate cycling supports methane and ethylene supersaturation in the phosphate-depleted western North Atlantic Ocean, Limnol Oceanogr, 65, 2443–2459, https://doi.org/10.1002/lno.11463, 2020.

Steinle, L., Graves, C., Treude,T., Ferre, B., Biastoch, A., Bussmann, I., Berndt, C., Krastel, S., James, R. H., Behrens, E., Böning, C.W., Greinert, J., Sapart, C-J., Scheinert, M., Sommer, S., Lehmann, Moritz F., Niemann, H., (2015): Methane concentration, oxidation rates and abundance of bacteria during Maria S. Merian cruise MSM21/4 at Svalbard seeps in summer 2012. PANGAEA, https://doi.org/10.1594/PANGAEA.844010, In supplement to: Steinle, L et al. (2015): Water column methanotrophy controlled by a rapid oceanographic switch. Nature Geoscience, 8(5), 378–382, https://doi.org/10.1038/ngeo2420

Stigebrandt, A. , 1984.: [15200485 - Journal of Physical Oceanography] The North Pacific_ A Global-Scale Estuary, n.d.

Sultan, N., Plaza-Faverola, A., Vadakkepuliyambatta, S., Buenz, S., and Knies, J.: Impact of tides and sea-level on deep-sea Arctic methane emissions, Nat Commun, 11, https://doi.org/10.1038/s41467-020-18899-3, 2020.

Tomczak, M. A multi-parameter extension of temperature/salinity diagram techniques for the analysis of non-isopycnal mixing. *Progress in Oceanography*, *10*, 147-171, 1981.

Torres-Valdés, S., Tsubouchi, T., Bacon, S., Naveira-Garabato, A. C., Sanders, R., McLaughlin, F. A., Petrie, B., Kattner, G., Azetsu-Scott, K., and Whitledge, T. E.: Export of nutrients from the Arctic Ocean, J Geophys Res Oceans, 118, 1625–1644, https://doi.org/10.1002/jgrc.20063, 2013.

Uhlig, C. and Loose, B.: Using stable isotopes and gas concentrations for independent constraints on microbial methane oxidation at Arctic Ocean temperatures, Limnol. Oceanogr.: Methods, 15, 737–751, https://doi.org/10.1594/PANGAEA.874893, 2017.

Uhlig, C., Kirkpatrick, J. B., D'Hondt, S., and Loose, B.: Methane-oxidizing seawater microbial communities from an Arctic shelf, Biogeosciences, 15, 3311–3329, https://doi.org/10.5194/bg-15-3311-2018, 2018.

Valentine, D. L.: Biogeochemistry and microbial ecology of methane oxidation in anoxic environments: a review, Antonie van Leeuwenhoek, 271–282 pp., 2002.

https://doi.org/10.5194/egusphere-2023-74
Preprint. Discussion started: 6 February 2023

Wang, Y., Yu, M., Austin, B., and Zhang, X. H.: Oleispira lenta sp. nov., a novel marine bacterium isolated from Yellow sea coastal seawater in Qingdao, China, Antonie van Leeuwenhoek, International Journal of General and Molecular Microbiology, 101, 787–794, https://doi.org/10.1007/s10482-011-9693-8, 2012.

Whiticar, M. J.: Carbon and hydrogen isotope systematics of bacterial formation and oxidation of methane, Chemical Geology, 291–314 pp., 1999.